SAPIENZA
UNIVERSITÀ DI ROMA

Inhomogeneous QCD phases at high baryonic potential

Facoltà di Scienze Matematiche, Fisiche e Naturali

Corso di Laurea Magistrale in Fisica

Candidate

Filippo Anzuini
ID number 1473314

Thesis Advisor

Prof. Omar Benhar Noccioli

Co-Advisors

Dr. Massimo Mannarelli
Dr. Stefano Carignano

Academic Year 2016/2017

Thesis not yet defended

Inhomogeneous QCD phases at high baryonic potential
Master thesis. Sapienza – University of Rome

This thesis has been typeset by LaTeX and the Sapthesis class.

Author's email: filippo.anzuini@gmail.com

Inhomogeneous QCD phases at high baryonic density

Filippo Anzuini

Contents

Chapter 1

Introduction - The QCD phase diagram

The QCD phase diagram has not been completely explored. While a chiral broken and confined phase is realized in the region corresponding to low temperatures T and low chemical potentials μ, when T is increased (and μ is kept substantially small), observational data from heavy nuclei collisions and lattice simulations supply the experimental and theoretical evidence of deconfined physics (see Fig 1.1). On the other hand, the low T and high μ region cannot be studied in a similar way: first of all, it is impossible to reproduce such extraordinary densities in laboratory; secondly, QCD can not be handled as a perturbative theory because, in the "intermediate region" for the chemical potential, quantum chromodynamics interactions are still characterized by a relatively strong coupling, which blows away the possibility of exploiting perturbative techniques; moreover, lattice calculations cannot be performed due to the sign problem [1, 4, 17].
In order to cope with such difficulties, usually effective models are used. They encode the main symmetries of full Quantum Chromodynamics in order to extract qualitative considerations about the quarks behavior for low temperatures and intermediate or high chemical potentials. It has already been proved how rich is the phenomenology that could be encountered in the QCD phase diagram characteristic of Neutron Stars (the intermediate regions) [1, 2, 4, 7, 17]: homogeneous and inhomogeneous chirally broken phases, an homogeneous color superconductor at higher chemical potentials and eventually a region of competition where inhomogeneous and homogeneous phases struggle one against the other [8, 17].

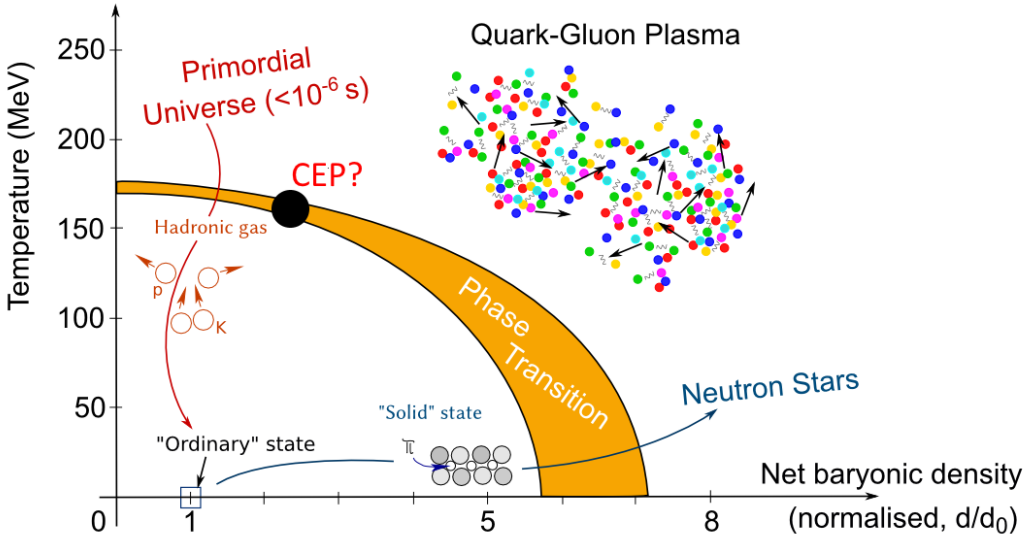

Figure 1.1: Representation of the QCD phase diagram. Antonin Maire, 2011, CERN.The critical end point (CEP) for QCD is where a second order phase transition is expected, as it is related to a first order phase transition line.

If we focus on the chemical potential axis (which corresponds to $T \simeq 0$), we can see how a phase transition separates a region where it it possible to find nuclear matter in the usual hadron gas/liquid state, from another one, in which the densities are so high that the bindings of the nuclei are weak and we can actually describe the relevant degrees of freedom in terms of quarks. Different authors [1, 5] have already underlined how this phase transition is expected to be first order (that is, the phase transition is characterized by a discontinuity of the free energy derivatives for some *critical* values of the thermodynamic variables). The phase transition line, starting from the abscissa axis, should end up in a second order critical point (or *CEP*, critical end point), where the first derivative of the free energy of the system is continuous, but the discontinuity is due to the second derivative, identifying a point where the function changes concavity, a flex point.
On the right of the first transition line we find a rich phenomenology, represented by the occurrence of chiral condensation and, at even higher density, of a color superconducting condensate.
Up to intermediate values of the chemical potential, the ground state of QCD is characterized by a chiral condensate, which comes from the coupling between a left-handed quark and a right-handed antiquark (and vice versa). The condensate that forms is homogeneous, independent of the spatial coordinates and so not spatially modulated. Nevertheless, it has been shown [16, 17] that allowing for a spatial modulation of this order parameter leads to the insurgence of a significant region of the QCD phase diagram where inhomogeneous condensates are favored with respect to homogeneous ones.

Chiral symmetry breaking is the symmetry breaking pattern whose outcome is the generation of a chiral order parameter given by the interaction between a quark and an antiquark with opposite chiralities.

We can start from the two flavor Lagrangian for quarks, observing that it possesses a global symmetry described by the SU(2) isospin group and its algebra. Nevertheless, we can broaden such symmetry when considering the chiral limit (massless quarks), as the quark Lagrangian is now invariant under non simultaneous symmetry transformations belonging to the product tensor group $SU(2)_L \otimes SU(2)_R$. Indeed, the free Dirac Lagrangian for up and down quarks is symmetric under two categories of transformations [6]:

$$q_R = U_R q = e^{-i\frac{\vec{\tau}}{2}\vec{\Theta}_R} q \qquad q_L = U_L q = e^{-i\gamma_5\frac{\vec{\tau}}{2}\vec{\Theta}_L} q \tag{1.1}$$

where q denotes the quark spinorial field and $\vec{\Theta}_{R/L}$ are respectively the right and left-handed chiral angles that rotate the quark spinors. When the Lagrangian is characterized by such invariance under global transformations, it possesses the chiral symmetry.
Equivalently, the left-handed and right-handed components for the quarks spinors can be obtained applying the chiral projectors

$$P_L = \frac{1-\gamma^5}{2} \qquad P_R = \frac{1+\gamma^5}{2} \tag{1.2}$$

to the quarks fields.
In vacuum, chiral symmetry breaking is characterized by the formation of an homogeneous condensate such that the expectation value is

$$\langle \bar{q}q \rangle = \langle \bar{q}_R q_L \rangle + \langle \bar{q}_L q_R \rangle \neq 0. \tag{1.3}$$

When we have a non-vanishing expectation value such as (1.3), it prevents the Lagrangian of the system to be invariant under global transformations acting separately on particles with opposite chiralities: the chiral symmetry is spontaneously broken, meaning that the symmetric properties of invariance under global transformation of the chiral symmetry groups are respected by the Hamiltonian but not by the ground state. Nevertheless, there is the possibility to reach a restoration of such symmetry at high temperature and density [6] .

A **color superconductor** is characterized by a qq interaction. Bardeen, Cooper and Schrieffer demonstrated that no free energy contribution is required for the formation of particle pairs at Fermi surfaces. Consequently, the presence of even the faintest attractive interaction between fermions on their common Fermi surface leads to the formation of couples of particles (Cooper pairs). The instability of Fermi surfaces of free fermions in high baryonic density systems makes the formation of Cooper pairs possible, but in the case of color superconductivity the interaction is driven by the attractive forces developed between two quarks, and the condensation generates a gap in the excitation spectrum. This characterizes in a peculiar way color superconductors from ordinary superconductors: while in the latter the attractive force driven by the ions in the lattice needs to overcome the repulsive interaction of two electrons to form a pair, quarks naturally interact among themselves through the strong force. As underlined in [2], the strong force can easily overcome the repulsion due to the electric interaction between quarks, and the condensate which characterizes color superconductivity is robust with respect to the typical Fermi

energy of such dense environments. The formation of a color superconductor has been already extensively analyzed by different authors [1, 2, 3, 4], as the excitation spectrum for deconfined matter could have a gap of $\mathcal{O}(100)$ MeV for values of the chemical potential μ that are expected in the inner regions of Neutron Stars. Nevertheless, in order to fully understand the potential impact that color superconductivity could have on physical observables for compact astrophysical objects, it is necessary to describe the QCD phase diagram corresponding to zero temperatures and intermediate/high values of the chemical potential.

At asymptotic baryonic density, the expected ground state is given by the *color-flavor-locked* (CFL) state. In this case, the density is such that a perturbative approach can be performed determining the properties of this color superconducting state [1, 2, 5]: the diquark condensate in the CFL phase is invariant under simultaneous transformations in flavor and color space. This is possible because, for very high values of the chemical potential μ, the strange quark mass can be neglected. Turning down the value of μ, the non vanishing value of the strange quark mass prevents the order parameter to preserve its $SU(3)$-flavor symmetry, and it could eventually disrupt the CFL phase for low values of μ.

The occurrence of color superconductivity in two-flavor systems is characterized by the presence of a non vanishing expectation value [1]

$$\langle q^T \mathcal{O} q \rangle, \tag{1.4}$$

where $\mathcal{O}$ denotes an operator in spinor, color and flavor spaces

$$\mathcal{O} = \mathcal{O}_{color} \otimes \mathcal{O}_{spinor} \otimes \mathcal{O}_{flavor} \tag{1.5}$$

and it needs to be antisymmetric. Indeed, for the Pauli exclusion Principle

$$q^T \mathcal{O} q = \mathcal{O}_{lm} q_l q_m = -\mathcal{O}_{lm} q_m q_l = -q^T \mathcal{O}^T q \longrightarrow \mathcal{O}^T = -\mathcal{O}. \tag{1.6}$$

The construction of such operator could follow many paths, and each of these represents a possible interaction between two different quarks that leads to the formation of the condensate. At asymptotic densities, the most attractive pattern for the interaction is the color-antitriplet channel for the diquark condensate. In full Quantum Chromodynamics this takes place exchanging a single gluon between quarks, while in effective models (that we shall adopt in this work) the interaction is modeled by a contact interaction. This determines the formation of a condensate of the form

$$z_{MM'} = \langle q^T i C \gamma_5 \tau_M \lambda_{M'} q \rangle, \tag{1.7}$$

where $\lambda_{M'}$ is a Gell-Mann matrix, τ_M is an isospin matrix belonging to the flavor space and C is the matrix of charge conjugation $C = i\gamma^2\gamma^0$.

We want to restrict the discussion to only two flavors and assume that the condensate is given by

$$z_{MM'} \longrightarrow z_{2,M'}. \tag{1.8}$$

Subsequently, we can rotate in color space the vector $z_{2,M'}$ exploiting a global color transformation and write

$$z_{22} = \langle q^T iC\gamma_5\tau_2\lambda_2 q\rangle. \tag{1.9}$$

It should be stressed that when only two quarks couple, the resulting state cannot be a color singlet state (but it is a *flavor* singlet, as we are considering only *up* and *down* quarks). When performing the global color rotation, we are assuming that the condensate involves only red and green quarks, while blue quarks do not condense.
Analyzing more in detail the symmetry properties of the 2SC condensate, we can write [4]

$$\langle qq\rangle_{2SC} \propto \epsilon_{ij}\epsilon^{abc}, \tag{1.10}$$

where $i, j = 1,2$ are the flavor indices for up and down quarks and $a, b, c = 1,2,3$ are the color indices. The condensate is antisymmetric in color space (indeed, the attractive channel for the condensation pattern is the antisymmetric antitriplet channel), it is antisymmetric in Dirac space (the quarks fields are spinors); as quarks need to obey to the Pauli exclusion principle, this imply that it must be a flavor singlet, *i.e.* antisymmetric also in flavor space.

1.1 Inhomogeneous color superconductivity and chiral condensates

When considering color superconductivity, pairs with null total momenta are favored above the ones with finite total momenta. Conversely, when certain conditions (as an high chemical potential) exert a stress over the Fermi surfaces, particles belonging to stressed (mismatched) surfaces need to spend part of their energy to couple. Since in such conditions the formation of couples with vanishing momenta is precluded by energetic considerations, diverse pairing patterns could be possibly explored, and certainly one of the most important allows the formation of pairs with a net momentum. In this way, an inhomogeneous condensate (space-dependent) is formed.
Crystalline color superconductivity (CSC) [5, 7] driven by the strong interaction between pairs of quarks involves a condensate which is spatially modulated as a crystal. When the radii of the Fermi surfaces are different, the creation of Cooper pairs requires an energetic cost proportional to $\delta\mu$, which represents the difference between the two chemical potentials of the two different species involved in the pairing. For small values of $\delta\mu$, the homogeneous BCS phase is still energetically favored. However, if $\delta\mu$ produces a critical stress on the BCS pairing, it is not energetically favored anymore for the system to generate an homogeneous condensate.
As an example, we can consider one of the simplest modulations, given by the LOFF structure, which assumes that the color superconductor condensate is given by a plane wave modulation (or a superposition of plane waves). In this case, the order parameter is spatially modulated as the pairing takes place between a quark with momentum k and another quark with a momentum equal to $-k + 2q$ [5]: this allows to both quarks to be

situated on their Fermi surfaces respectively, while allowing them to couple with a resulting modulation characterized by a total momentum given by $2q$, whose magnitude is given by the relative distance between the two species Fermi surfaces. While in the BCS mechanism the formation of Cooper pairs can take place over all the Fermi surfaces, in general the possibility of a coupling for inhomogeneous condensates is restricted to smaller regions (more precisely to *rings*) across the Fermi surfaces. Indeed, as one quark has a momentum equal to k and the other one equal to $-k + 2q$, the two quarks would reside on two antipodal rings, and their Fermi surfaces will be separated by a radius of the order of q. The regions where the coupling cannot happen are called *blocking regions*; they host a species of quarks with a specific momentum which is not possessed by the other species, and this would prevent the condensation.
Considering inhomogeneous chiral symmetry breaking in high baryonic density systems, a spatially modulated order parameter is the result of the split of the respective Fermi surfaces for particles and antiparticles. Indeed, if for low chemical potentials homogeneous phases are due to the coupling of quarks and antiquarks, when we consider higher μ the energy required to form a couple $\bar{q}q$ is at least given by 2μ, because Fermi surfaces for particles and antiparticles are strayed as a consequence of the different chemical potential for the two species. As an aftermath, particle-hole pairing patterns could be explored instead of quark-antiquark ones: indeed, being energetically too expensive to excite antiparticles at high baryonic potentials, the pairing pattern passes through the formation of quark-hole pairs, as both quarks and holes involved in the pairing pattern could reside on their common Fermi surface. In this case, the pairs would carry a total finite momentum given by the sum of the two momenta.
Different authors [1, 8, 17] have already shown that there is a region in the QCD phase diagram where a competition between an inhomogeneous chiral condensate and a color superconductor is expected and that divides the chirally broken, homogeneous phase and the homogeneous 2SC phase. Indeed, if we allow [8] for both the interactions in the quark-antiquark and in the diquark channel, considering a spatial modulation only for the chiral condensate (in the form of a cosine for simplicity) while assuming that the color superconductor, given by a 2SC condensate, is homogeneous, the numerical minimization of the free energy depicts the presence of a region at intermediate chemical potential (300 MeV $< \mu <$ 350 MeV) where the favored state from an energetic point of view is given by the presence of non-vanishing expectation value for both condensates. For higher values of the chemical potential, the parameters that describe the chiral condensate vanish, and only a 2SC color superconductor is expected, in accordance with the usual picture of a superconducting phase for deconfined quark matter at very high baryonic densities.
We argue that the fact that only one of the order parameters is spatially modulated is due to the impossibility of considering both condensates to be space dependent, as this complicates in an enormous way the diagonalization of the hamiltonian matrix.
Nevertheless, we will show that exploiting the perturbation theory and adopting a qualitative approximation for the chiral condensate contribution to the free energy, we are able to reproduce a spatial modulation also for the diquark condensate: indeed, if we consider in the region 300 MeV $< \mu <$ 350 MeV that the 2SC phase is characterized by a small

expectation value while the chiral condensate is much more relevant, we are able to reproduce such competition between the two phases, where the chiral condensate forces an inhomogeneous 2SC order parameter to have its maxima where the chiral condensate has its minima.

1.2 Phenomenology

As discussed in numerous works [2, 3, 7], the realization of chiral and color superconductive condensates is thought to thrive in Neutron Stars or, more in general, in compact astrophysical objects whose densities would be well above the nuclear saturation densities. Nevertheless, whether such condensation patterns would happen or not is still unclear, as the expected consequences of chiral and color superconducting phases would take place in compact stars core, and the aftermaths of such presence could be masked by the intermediate layers of such astrophysical objects that, conversely, are composed by standard nuclear matter. Actually, a clear signature of the occurrence of quark deconfinement has not been observed yet.

1.2.1 Neutron Stars

As the thermal energy generated in the core of a star is not able to sustain anymore the gravitational force, the outer layers of the star begin to fall on the core [9]. If its mass is in the range from $\sim 8M_{\odot}$ to $20/30M_{\odot}$, the nuclear matter confined in the core hosts thermonuclear reactions which can synthesize all the elements until ^{56}Fe is generated. The core si destabilized by different processes, as the escape of neutrinos or the photodisintegration of the synthesized iron. As the core mass exceeds the Chandrasekhar limit, the internal gradient pressure can no longer balance the gravitational collapse. In this compression process, extraordinary densities can be reached by the core, easily exceeding the density of atomic nuclei; eventually, the outer layers are blown away by the shock waves produced by the collapse, exploding in a supernova.
The central object, which is defined as the *remnant* of such process, is a Neutron Star, whose structure is subdivided in different layers with typical solidnesses:

- Outer crust ($\sim 0.5km$). The density of the outer crust is in the range of $10^7 g/cm^3 \leq \rho \leq 4 \times 10^{11} g/cm^3$. The matter is composed of an electron gas and a lattice of heavy nuclei. As the density increases in the most internal layers, neutrons start to drip out of the nuclei.

- Inner crust ($\sim 1km$). In this region, a rich phenomenology is expected for nuclear matter. The density ranges from $4 \times 10^{11} g/cm^3$ up to $2.67 \times 10^{14} g/cm^3$.

- Core ($\sim 10km$). The density increases from the value of $2.67 \times 10^{14} g/cm^3$ to at least $10^{15} g/cm^3$. It is still unclear the composition of the core. Some suggest that heavy hyperons could be produced to minimize the internal energy of nuclear matter; nevertheless, at such densities, the occurrence of quark deconfinement could actually take place, giving birth to a rich phenomenology, involving chiral and color superconducting condensates.

It is extremely difficult to infer the effective composition of a Neutron Star core, as the observable effects that heavy hyperons and deconfined quarks could produce are very faint.

Pulsar glitches

Pulsar glitches are observed as a sudden, slight increase of Neutron Stars angular velocity. The complexity of such phenomenon requires a noticeable theoretical and computational effort. The standard glitch mechanism assumes that the radiation emission makes the pulsar lose part of its angular velocity while the inner superfluid spins faster than the outer crust. Given the fact that its vortices are quantized and bound to specific sites of the crust, the superfluid cannot spin down. When the different spin velocities reach a critical value, the vortices unpin from their original sites leading to a sudden increase of the pulsar crust angular rotation.
Two phases of pulsar glitches can be inferred from observational data: the spin-up phase (led by the unpinning of the quantized vortices) and a spin-down phase (distinguished by the corotation restoration of the superfluid with the crust). The analysis of this second stage with different models (see [10] for example) and the fit of the spin frequency with observational data allow to determine important quantities characterizing the superfluid, such as viscosity, stratification and compressibility. Despite this, these models are unable to include the different timescales of the spin-down phase that are observed between the glitches in the same pulsar. This is caused by the global nature of the mechanism that underlies the glitches: the unpinning across the star interior of many of the quantized vortices from their original sites. In addition to this, the various models can hardly take into account the presence of a core and the interplay between the different components of the fluid (neutral and charged particles), which are expected to be crucial for the glitch dynamics.
Furthermore, the flow that causes such glitches is likely to be non-axisymmetric; indeed, it can determine a quadrupole moment which would allow the system to emit Gravitational Waves (GW). From the amplitude of the signal it is possible to infer constraints over the fluid model parameters. In this way, Gravitational Waves could be exploited as an effective tool to model the Neutron Stars internal mechanism that leads to the production of a glitch, as in [12].
Despite the theoretical effort to model the complex mechanisms of pulsar glitches, a new interpretation to pulsar glitches is required, including superfluid neutral and charged components interactions and relevant physical features that are expected in the inner regions of Neutron Star, as the occurrence of quark deconfinement and heavy hyperons. The detection of isolated Neutron Stars gravitational signals in the form of GW will unveil fundamental internal properties characteristic of these compact objects, as gravitational waves can be related with fundamental quantities characterizing the Neutron Stars structure.

This work is organized as follows: in Chapter 2 we will describe the problem of the diagonalization of the Hamiltonian for the inhomogeneous chiral condensate, explaining why it is necessary to develop an approximate method that could describe the grand potential of

this phase. We will introduce such method on a qualitative level, and we will show how in this case it is possible to consider both the chiral and the 2SC condensate as inhomogeneous. In Chapter 4 instead, we will obtain a rigorous expansion for the thermodynamic potential with which we will be able to describe the free energies for inhomogeneous chiral condensates for every value of the chemical potential in the range 300 MeV $< \mu <$ 345 MeV, which is relevant for Neutron Stars cores.

Chapter 2

Eigenvalue problem and qualitative Thomas-Fermi approximation

2.1 The Nambu-Jona Lasinio model

The Nambu-Jona Lasinio model [13, 14] was introduced in 1961 to describe the generation of a gap (dynamical mass) through a contact interaction between nucleons. Indeed, the self-energies terms in the perturbative approach induce the presence of a non-vanishing effective mass M even in the chiral limit.
Subsequently, the model was exploited in QCD reinterpreting the spinor fields as quarks, carrying spinor, flavor and color indices. It should be stressed that the model is non renormalizable, that it does not include gauge bosons (*gluons*) and that the coupling constant is effectively constant: it does not change as the running coupling constant of full QCD. The model preserves the chiral symmetry of the theory but, due to its nature, it does not describe confinement physics.
The Nambu-Jona Lasinio Lagrangian is given by

$$\mathcal{L} = \bar{q}(i\gamma^{\mu}\partial_{\mu} - \tilde{m})q + G[(\bar{q}q)^2 + (\bar{q}i\gamma^5\vec{\tau}q)^2], \tag{2.1}$$

where q are the quark spinors and the Dirac, flavor and color indices have been suppressed for simplicity. We are assuming that the quarks involved in the interaction are the *up* and *down* quarks, which have three colors: *blue*, *red* and *green*. The first term in the above expression is the free Lagrangian while the second term involves the coupling of the quarks through a contact interaction represented by the G coupling constant, which is the same for the scalar $\bar{q}q$ and the pseudoscalar $\bar{q}i\gamma^5\vec{\tau}q$ interactions terms and which has dimensions E^{-2}: this signals that the model is not renormalizable, and it implies that in order to eliminate the occurring divergencies, a regularization prescription should be included in the model [18]. The γ^5 matrix is the fifth Dirac matrix acting on the Dirac indices, while the $\vec{\tau}$ matrix is the Pauli matrix acting on the flavor indices. Eventually, the mass matrix $\tilde{m}$ contains the bare masses of the *up* and *down* quarks, which are assumed to be the same. From (2.1) it is possible to obtain the grand potential Ω

$$\Omega(T,\mu) = -\frac{T}{V} log[Z(T,\mu)],$$

where $Z(T,\mu)$ represents the partition function whose explicit expression [19] is

$$Z(T,\mu) = \int d[\bar{q}]d[q] exp\Big(\int_{V_4} d^4x_E \big[\mathcal{L}_{NJL} + \mu\bar{q}\gamma^0 q\big]\Big) \tag{2.2}$$

with the four-volume integral domain $V_4 = \frac{1}{T} \times V$, where T is the temperature and V is the 3D space volume, being the integral performed in Euclidean space.
We will use throughout this work the mean field approximation, in which the condensates are represented by their expectation values neglecting their fluctuations around the mean value. Denoting with ϕ_s and ϕ_p^i the scalar and the pseudoscalar condensates expectation values

$$\langle\bar{q}q\rangle = \phi_s \qquad \langle\bar{q}i\gamma^5\tau^i q\rangle = \phi_p^i, \tag{2.3}$$

we can rewrite the NJL Lagrangian in the form

$$\mathcal{L}_{MF} = \bar{q}\Sigma^{-1}q - \mathcal{V}$$

where Σ^{-1} is the inverse propagator in position space

$$\Sigma^{-1} = i\gamma^\mu\partial_\mu - m + 2G(\phi_s + i\gamma^5\phi_p^i)$$

and

$$\mathcal{V} = G[\phi_s^2 + (\phi_p^i)^2].$$

Furthermore, we will consider only the pseudoscalar condensate pointing in the third direction of the isospin space (it is possible to generalize it considering a global rotation transformation in isospin space), so that

$$\phi_p^i = \delta_{i,3}\phi_p^3$$

and, for simplicity, we rewrite ϕ_p^3 as ϕ_p. If we assume that the condensate, instead of being homogeneous, is space dependent, we can write

$$\phi_s \longrightarrow \phi_s(\vec{x}) \qquad \phi_p \longrightarrow \phi_p(\vec{x}), \tag{2.4}$$

where we have excluded the possibility for both condensates to be time-dependent. It should be stressed that in general it is not feasible even a numerical analysis of such systems if they are allowed to have a 3D spatial modulation; indeed, it is not possible to diagonalize the Hamiltonian.
We introduce an effective inhomogeneous mass function given by

$$M(\vec{x}) = m - 2G(\phi_s(\vec{x}) + i\phi_p(\vec{x})) \tag{2.5}$$

and the inverse propagator in coordinate space takes the form

$$\Sigma^{-1}(\vec{x}) = i\gamma^{\mu}\partial_{\mu} - M(\vec{x}). \tag{2.6}$$

In order to obtain the energy spectrum for the system of quarks we write the explicit expression of the Hamiltonian

$$\mathcal{H}(\vec{x}) = \gamma^0[-i\gamma^i\partial_i + M(\vec{x})], \tag{2.7}$$

and so we can obtain the propagator expressed as

$$\Sigma^{-1}(\vec{x}) = \gamma^0(i\partial_0 - \mathcal{H}(\vec{x})). \tag{2.8}$$

Now it is convenient to exploit the chiral representation introducing the bi-spinor $\chi(p)$

$$\chi = \begin{bmatrix} P_L q \\ \\ P_R q \end{bmatrix}, \tag{2.9}$$

where P_L and P_R are the projection operators. In this way, it is possible to separate the Hamiltonian

$$\mathcal{H}(\vec{x}) = \mathcal{H}(\vec{x})_+ \otimes \mathcal{H}(\vec{x})_-$$

but actually we can restrict ourselves to $\mathcal{H}_+$, as if we were dealing only with particles but not antiparticles; indeed, the two sub-Hamiltonians have the same energy spectrum. Expressing $\mathcal{H}_+$ on the chiral basis we can write

$$\mathcal{H}_+ = \begin{bmatrix} i\sigma^i\partial_i & M(\vec{x}) \\ \\ M^*(\vec{x}) & -i\sigma^i\partial_i \end{bmatrix}. \tag{2.10}$$

In order to obtain the eigenvalues spectrum of this Hamiltonian, it is possible to handle the problem only for periodic modulations of the chiral condensate, so assuming it could be expanded through a Fourier series in such a way that

$$M(\vec{x}) = \sum_{\vec{Q}_i} M_{\vec{Q}_i} e^{i\vec{Q}_i\cdot\vec{x}}. \tag{2.11}$$

We can write the Fourier transform of the Hamiltonian in momentum space as

$$\mathcal{H}_{\vec{p_l},\vec{p_m}} = \frac{1}{V}\int d^3x e^{-i\vec{p}_l\cdot\vec{x}}\mathcal{H}_+ e^{i\vec{p}_m\cdot\vec{x}} = \begin{bmatrix} -\vec{\sigma}\cdot\vec{p}_m\delta_{\vec{p}_l-\vec{p}_m} & \sum_{Q_i} M_{\vec{Q}_i}\delta_{\vec{p}_m-\vec{p}_l-\vec{Q}_i} \\ \\ \sum_{Q_i} M^*_{\vec{Q}_i}\delta_{\vec{p}_m-\vec{p}_l+\vec{Q}_i} & \vec{\sigma}\cdot\vec{p}_m\delta_{\vec{p}_l-\vec{p}_m} \end{bmatrix}. \tag{2.12}$$

This is a matrix which is non diagonal and, furthermore, it is infinite in momentum space. In the following we illustrate some methods to handle this Hamiltonian.

2.1.1 Boosting method

Following [15, 16, 17], we introduce the basics of the boosting method for one-dimensional modulations. Exploiting the Lorentz symmetries of the problem, it is possible indeed to simplify the eigenvalue problem of the Hamiltonian.
Suppose we have a Lorentz transformation representation given by $S(\Lambda)$, and let us denote the momentum operator for the free spinors as $P^\mu = (H, P_i)$. We can write

$$S(\Lambda)P^\mu S^{-1}(\Lambda) = \Lambda^\mu_\nu P^\nu. \tag{2.13}$$

It is obvious that when we consider condensates that depend on the spatial coordinates, the system is no longer invariant under translations in those directions. Nevertheless, if we consider, as an example, 1D modulations, the momentum operator $P_\perp$ commutes with the Hamiltonian of the system, meaning that it preserves the translational invariance along the directions which are orthogonal to the condensate modulation. This commutativity between $P_\perp$ and $\mathcal{H}$ implies that the common eigenstates have to be labeled with the eigenvalues corresponding to $P_\perp$.
If we consider the eigenstates of $\mathcal{H}$ such that

$$\mathcal{H}q_{\lambda,0} = \lambda q_{\lambda,0} \qquad P_\perp q_{\lambda,0} = 0 \tag{2.14}$$

and if Λ^μ_ν is the matrix representation of the Lorentz transformation such that $(\lambda, 0)^\mu$ is transformed into $\left(\lambda\sqrt{1+\mathbf{p}_\perp/\lambda^2}, \mathbf{p}_\perp\right)^\mu$, imposing that

$$q_{\lambda\sqrt{1+\mathbf{p}_\perp/\lambda^2},\mathbf{p}_\perp} = \left(\sqrt{1+\mathbf{p}_\perp/\lambda^2}\right)^{-\frac{1}{2}} S^{-1}(\Lambda)q_{\lambda,0} \tag{2.15}$$

it is possible to verify that

$$P^\mu q_{\lambda\sqrt{1+\mathbf{p}_\perp/\lambda^2},\mathbf{p}_\perp} = \left(\lambda\sqrt{1+\mathbf{p}_\perp/\lambda^2}, \mathbf{p}_\perp\right)^\mu q_{\lambda,0}. \tag{2.16}$$

Thus, the energy spectrum of the system can be constructed considering a reference frame in which transverse momenta are null. Then, for any value of $p_\perp$, the eigenvalues can be obtained by a boost.
Choosing a 1D modulation, in coordinate space we have

$$\mathcal{H} = \begin{bmatrix} i\partial_z & 0 & M(z) & 0 \\ 0 & -i\partial_z & 0 & M(z) \\ M^*(z) & 0 & -i\partial_z & 0 \\ 0 & M^*(z) & 0 & i\partial_z \end{bmatrix}, \tag{2.17}$$

where we have explicitly shown the Dirac structure of the matrix. Considering simple modulations would make the eigenvalue problem less complicated. For example, as shown in [16], we can choose the modulation as

$$M(z) = 2Mcos(Qz), \tag{2.18}$$

where we assume that M is a constant amplitude. Substituting this expression in (2.12) we get

$$\begin{aligned}\mathcal{H}^{+}_{p_i,p_j} =& \frac{1}{V}\int dz e^{-ip_j z}\gamma^0[-i\gamma^3\partial_z + M(e^{iQz}+e^{-iQz})]e^{ip_i z} = \\ &= \frac{1}{V}\int dz\gamma^0[e^{-i(p_j-p_i)z}\gamma^3 p_i + M(e^{-i(p_j-Q-p_i)}+e^{-i(p_j+Q-p_i)})] = \\ &= \gamma^0[\gamma^3 p_i\delta_{p_i,p_j} + M(\delta_{p_j,p_i+Q}+\delta_{p_j,p_i-Q})],\end{aligned} \tag{2.19}$$

where p_i, p_j are two generic momenta in the z direction. We can see how an inhomogeneous condensate radically complicates the structure of the Hamiltonian. Indeed, two generic momenta are coupled through the presence of the Kronecker delta functions due to the presence of the condensate. Considering the coupling between two momenta (p_1 and p_2 oriented along the z axis) we have the following blocks

$$\begin{aligned}\mathcal{H}_{p_1,p_1} &= \gamma^0[\gamma^3 p_1\delta_{p_1,p_1} + M\delta_{p_1,p_1+Q} + M\delta_{p_1,p_1-Q}], \\ \mathcal{H}_{p_1,p_2} &= \gamma^0[M\delta_{p_1,p_2+Q} + M\delta_{p_1,p_2-Q}], \\ \mathcal{H}_{p_2,p_1} &= \gamma^0[M\delta_{p_2,p_1+Q} + M\delta_{p_2,p_1-Q}], \\ \mathcal{H}_{p_2,p_2} &= \gamma^0[\gamma^3 p_1\delta_{p_2,p_2} + M\delta_{p_2,p_2+Q} + M\delta_{p_2,p_2-Q}].\end{aligned} \tag{2.20}$$

Exploiting the analogy with crystalline periodic structures in condensed matter physics (indeed, we are considering periodic modulations), we can express the generic momentum p_j as a sum of a wavevector in the First Brillouin Zone (IBZ) plus a vector that reflects the periodicity of our problem (in our case, this is represented by Q). In this way, we can write $p_j = k + jQ$, where k denotes a vector belonging to the IBZ. In conclusion, the momenta that couple are the ones that differ of a reciprocal lattice vector, which defines the periodic structure of the condensate in the reciprocal space.
We want to make use of the boosting method expressing the hamiltonian matrix in a reference frame where the transverse momenta are null. Performing an unitary transformation over (2.17) we can obtain a matrix (in coordinate space) of the form

$$\mathcal{H} = \begin{bmatrix} -i\partial_z & M(z) & 0 & 0 \\ M^*(z) & i\partial_z & 0 & 0 \\ 0 & 0 & -i\partial_z & M^*(z) \\ 0 & 0 & M(z) & i\partial_z \end{bmatrix}. \tag{2.21}$$

Let us consider only the upper block

$$\mathcal{H}_{up} = \begin{bmatrix} -i\partial_z & M(z) \\ M^*(z) & i\partial_z \end{bmatrix} \tag{2.22}$$

and the coupling of two momenta only (say $p_1 = k + Q$ and $p_2 = k + 2Q$). Using the Fourier expansion (2.11) and limiting ourselves to 1D modulations involving only ± 1 harmonics, the general structure of $\mathcal{H}_{up}$ in momentum space is given by

$$\mathcal{H}^{up}_{p_1,p_2} = \begin{bmatrix} H_{11} & H_{12} \\ H_{21} & H_{22} \end{bmatrix} = \tag{2.23}$$

$$\begin{bmatrix} p_1\delta_{1,1} & M_Q\delta_{1,1+Q} + M_{-Q}\delta_{1,1-Q} & p_1\delta_{1,2} & M_Q\delta_{1,2+Q} + M_{-Q}\delta_{1,2-Q} \\ M^*_{-Q}\delta_{1,1-Q} + M^*_Q\delta_{1,1+Q} & -p_1\delta_{1,1} & M^*_{-Q}\delta_{1,2-Q} + M^*_Q\delta_{1,2+Q} & p_1\delta_{1,2} \\ p_2\delta_{2,1} & M_Q\delta_{2,1+Q} + M_{-Q}\delta_{2,1-Q} & p_2\delta_{2,2} & M_Q\delta_{2,2+Q} + M_{-Q}\delta_{2,2-Q} \\ M^*_{-Q}\delta_{2,1-Q} + M^*_Q\delta_{2,1+Q} & p_2\delta_{2,1} & M^*_{-Q}\delta_{2,2-Q} + M^*_Q\delta_{2,2+Q} & -p_2\delta_{2,2} \end{bmatrix}$$

where $\delta_{i,j} \equiv \delta_{p_i,p_j}$ and assuming that $M_Q = M_{-Q}$ we have

$$\begin{bmatrix} p_1\delta_{1,1} & 0 & 0 & M_Q\delta_{1,2-Q} \\ 0 & -p_1\delta_{1,1} & M^*_Q\delta_{1,2-Q} & 0 \\ 0 & M_Q\delta_{2,1+Q} & p_2\delta_{2,2} & 0 \\ M^*_Q\delta_{2,1+Q} & 0 & 0 & -p_2\delta_{2,2} \end{bmatrix}. \tag{2.24}$$

We can obtain the eigenvalues of such matrix after a little of algebra:

$$\begin{aligned} 0 = det(\mathcal{H}^{up}_{p_1,p_2} - \lambda\mathbb{1}) = \sum_{i=1}^{D}(-1)^{i+j} det(H_{ij} - \lambda_{ii}) = \\ = -(p_1 - \lambda)(p_2 + \lambda)[-(p_1 + \lambda)(p_2 - \lambda) - |M_{Q_1}|^2] \\ - |M_{Q_1}|^2[-(p_1 + \lambda)(p_2 - \lambda) - |M_{Q_1}|^2] \end{aligned} \tag{2.25}$$

where we imposed $Q = p_1 - p_2 \equiv Q_1$.

The four eigenvalues are

$$\begin{aligned} \lambda_1 &= -\frac{1}{2}\Big(\sqrt{4|M_{Q_1}|^2 + (p_1 + p_2)^2} + p_1 - p_2\Big), \\ \lambda_2 &= -\frac{1}{2}\Big(\sqrt{4|M_{Q_1}|^2 + (p_1 + p_2)^2} - p_1 + p_2\Big), \\ \lambda_3 &= +\frac{1}{2}\Big(\sqrt{4|M_{Q_1}|^2 + (p_1 + p_2)^2} + p_1 - p_2\Big), \\ \lambda_4 &= +\frac{1}{2}\Big(\sqrt{4|M_{Q_1}|^2 + (p_1 + p_2)^2} - p_1 + p_2\Big). \end{aligned} \tag{2.26}$$

It is still difficult to diagonalize the Hamiltonian, although we are now coupling just two momenta separated by a reciprocal lattice vector. In a more general situation, this coupling is not restricted just to p_1 and p_2. In the "full" problem, we would get a matrix $\mathcal{H}(k)$ for each wavevector of the First Brillouin Zone, and each $\mathcal{H}(k)$ is a matrix where k is coupled to $k \pm Q, k \pm 2Q, ..., k \pm NQ$. The general method to handle the diagonalization of such kind of matrices is to perform a numerical computation of the eigenvalues imposing a cutoff Λ (limiting in this way the allowed couplings of quarks which differ of a reciprocal lattice vector jQ) [16, 17].

2.2 Thomas-Fermi approximation

The *Density Functional Theory* (DFT) has been originally developed to describe the behavior of interacting electrons in an external potential: it allows a drastic simplification of such complex dynamics, as it is necessary to determine only the ground state density to obtain all the relevant quantities of the system. The rationale of the DFT method hinges on the Hohenberg-Kohn theorem, whose statement establishes a univocal relation between the expectation value of any operator and the ground state density. Although the enormous simplification, the theorem does not give any clue on how to determine such density. The Thomas-Fermi method is a semi-classical approximation used to describe the spatial distribution of the electronic cloud surrounding heavy nuclei. It describes the kinetic energy and the electron-electron mutual interaction as a function of the number density deduced from simple considerations on the volume occupied by N particles in the phase space. Assuming that the maximum momentum is given by the Fermi momentum p_F, the distribution of electrons is assumed to be locally uniform in space volumes V. Still, the number density is position-dependent.

We want to explore in this chapter whether the Thomas-Fermi approximation could be a valid tool to curtail the difficulties encountered with the eigenvalue problem for the chiral condensate. Furthermore, our true aim is to investigate the competion between the chiral condensate and the 2SC diquark condensate, both spatially modulated. Analytic solutions are not an option in this situation, and even a numerical computation is not feasible. It is obvious that it is important to determine the validity or not of approximation methods that could describe the grand potential for inhomogeneous phases in order to study the thermodynamic properties of quark matter where both the order parameters are taken into account. Nevertheless, we want to underline that in this chapter the results that we will obtain need to be considered on a qualitative level; indeed, we will use the Thomas-Fermi approximation and then we will apply correction terms actually *forcing* the grand potential obtained with this method to reproduce the results of the *numerical* problem obtained in [16, 17]. Our aim in this chapter is just to obtain a suitable, analytic expression of the grand potential for the chiral condensate and to outline a perturbative approach through which we can add an inhomogeneous 2SC condensate. In Chapter 4, instead, we will outline a rigorous derivation for the grand potential that will not hinge on previous results based on the hamiltonian diagonalization, and we will obtain an analytic expression for the grand potential such that we will be able to reproduce the results of the

numerical problem in every region of the QCD phase diagram at $T = 0$.
In this Chapter, we will first write the free energy that describes the homogeneous phase and the one for the restored phase, which is reached when the order parameter tends to zero. After that, we will define our qualitative Thomas-Fermi approximation. We will work in the chiral limit (massless quarks).
Since the expression of the thermodynamic potential needs to be regularized, we will exploit the Pauli-Villars regularization scheme.

2.2.1 Pauli-Villars regularization scheme

The explicit form of the thermodynamic potential is given by the sum of a kinetic term and a condensate contribution. For the kinetic term (in which are present both the vacuum and the medium contribution), we have [16, 17]

$$\Omega_K = -2N_c \int_{IBZ} \frac{d^3k}{(2\pi)^3} \sum_{\lambda} \Big[\frac{E_\lambda(\vec{k}) - \mu}{2} + T \log\Big(1 + e^{-\frac{E_\lambda(\vec{k})-\mu}{T}}\Big)\Big], \tag{2.27}$$

where with $E_\lambda(\vec{k})$ we indicate the eigenvalues for homogeneous phases. If the spectrum is symmetric around the origin, we can expand the kinetic contribution

$$\Omega_K = -2N_c \int_{IBZ} \frac{d^3k}{(2\pi)^3} \sum_{\lambda>0} \Big[E_\lambda(\vec{k}) + T \log\Big(1+e^{-\frac{E_\lambda(\vec{k})-\mu}{T}}\Big) + T \log\Big(1+e^{-\frac{E_\lambda(\vec{k})+\mu}{T}}\Big)\Big], \tag{2.28}$$

where we are considering only the positive eigenvalues. We can separate the two different contributions given by the vacuum and the medium terms inside the previous expression, rearranging the terms [16] in such a way that

$$\begin{aligned}
\Omega_K &= -2N_c \int_{IBZ} \frac{d^3k}{(2\pi)^3} \sum_{\lambda>0} \Big[E_\lambda(\vec{k}) + T \log\Big(1 + e^{-\frac{E_\lambda(\vec{k})-\mu}{T}}\Big) + T \log\Big(1 + e^{-\frac{E_\lambda(\vec{k})+\mu}{T}}\Big)\Big] \\
&= -2N_c \int_{IBZ} \frac{d^3k}{(2\pi)^3} \sum_{\lambda>0} \Big[E_\lambda(\vec{k}) + T \log\{\Big(1 + e^{-\frac{E_\lambda(\vec{k})-\mu}{T}}\Big)\Big(1 + e^{-\frac{E_\lambda(\vec{k})+\mu}{T}}\Big)\}\Big] \\
&= \Omega_{vac} + \Omega_{med}.
\end{aligned} \tag{2.29}$$

Taking the limit for $T \to 0$ we can see how the medium contribution Ω_{med} reduces to

$$\lim_{T\to 0} \Omega_{med} = -2N_c \int_{IBZ} \frac{d^3k}{(2\pi)^3} \sum_{\lambda>0} \Big[(\mu - E_\lambda(\vec{k}))\theta(\mu - E_\lambda(\vec{k}))\Big]. \tag{2.30}$$

As a note to this limit, we underline that after a few seconds after their birth, Neutron Stars are characterized by a temperature which is below a few keV, therefore much below

the energy scales considered here [7].
The condensate contribution instead is given by

$$\Omega_{cond} = \frac{1}{4G}\sum_{\vec{Q}} |M_{\vec{Q}}|^2, \tag{2.31}$$

and it is evident how the medium and the condensate parts are not potentially divergent. On the other hand, the vacuum contribution needs to be regularized. The Pauli-Villars regularization scheme [17, 18] consists in substituting the eigenvalues as follows

$$E \to \qquad \sum_{j=0}^{3} c_a \sqrt{E^2 + j\Lambda_{PV}^2}, \tag{2.32}$$

where the coefficients of the Pauli-Villars regularization method are given by $c_{PV}(0) = 1$, $c_{PV}(1) = -3$, $c_{PV}(2) = 3$, $c_{PV}(3) = -1$, while Λ_{PV} is the energy cut off. Adopting this regularization scheme

$$\Omega_{vac} = -\frac{2N_f N_c}{(2\pi)^3}\sum_{j=0}^{3}\int d^3p \Big[c_{PV}(j)\sqrt{E_{hom}^2 + j\Lambda_{PV}^2}\Big], \tag{2.33}$$

where $E_{hom} = \sqrt{p^2 + M^2}$.
The grand potential for the restored phase, Ω_{rest}, is obtained by taking the limit for $M \to 0$.

2.2.2 Chiral condensate - Ω_{TF}

We now outline the Thomas-Fermi approximation in order to describe the grand potential for inhomogeneous phases. As it has already been shown in previous works [15, 16, 17], the favored spatially-dependent phase is described by a one-dimensional solitonic-like modulation, expressed in terms of Jacobi elliptic functions

$$M(z) = \Delta\nu \frac{sn(\Delta z|\nu)cn(\Delta z|\nu)}{dn(\Delta z|\nu)}, \tag{2.34}$$

where sn, cn and dn are respectively the elliptic sine, the elliptic cosine and the delta amplitude and whose period is given by

$$L(\Delta, \nu) = 2\frac{\mathcal{K}(\nu)}{\Delta}, \tag{2.35}$$

where $\mathcal{K}(\nu)$ is a complete elliptic integral of first kind and $\nu \in [0,1]$ is the elliptic modulus. The solitonic solution to the eigenvalue problem is characterized by two parameters, Δ and ν. When we take the limit $\nu \to 1$, the periodic modulation reduces to a single kink, because it reduces to an hyperbolic tangent. On the opposite, when decreasing the value of ν, the shape of the mass function reduces to a sinusoidal modulation as shown in Fig 2.1

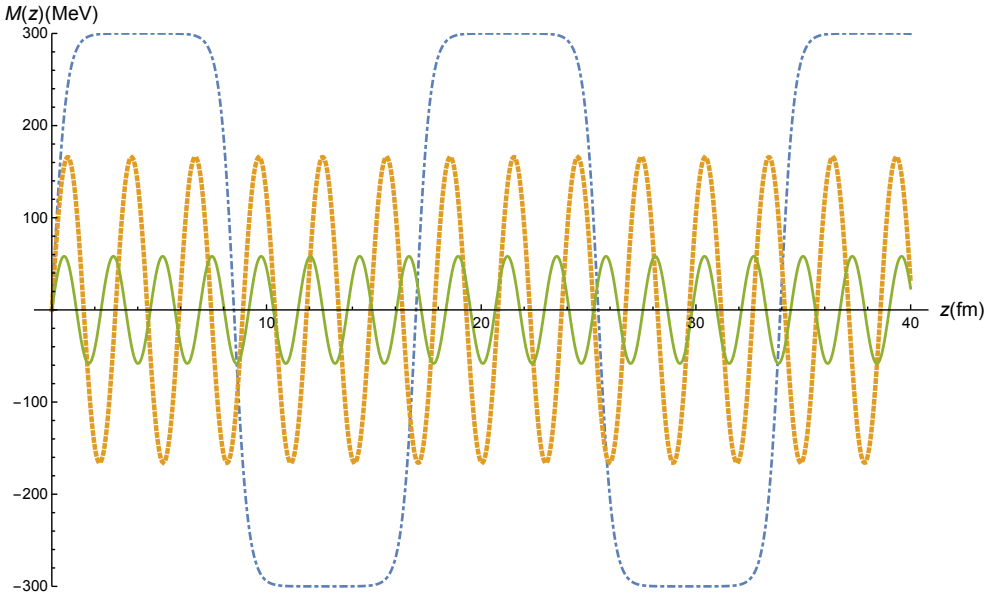

Figure 2.1: Plot of the modulation $M(z)$ (eq.(2.34)) for different values of the elliptic parameter ν. The dot dashed (blue) line represents the solitonic modulation for $\nu = 0.999$. The dashed (yellow) line is for $\nu = 0.8$ while the solid line is for $\nu = 0.35$.

Considering this modulation for the effective mass characterizing the chiral condensate, the qualitative Ω_{TF_0} approximation will be determined as follows :

- we substitute in Ω_{hom} the homogeneous parameter M with the solitonic modulation $M(z)$. With such procedure, the grand potential is now dependent from the z-coordinate. We define $\Omega_{TF_0}(z) = \Omega_{hom}(M(z))$.

- we average the $\Omega_{TF_0}(z)$ over the dimension of a linear cell, which is determined by the period of the spatially-dependent condensate. In this way, we obtain the mean value of $\langle\Omega_{TF_0}(z)\rangle$ over a period of the modulation.

As a first check, we verify that, in the limit of $M \to 0$, $\langle\Omega_{TF_0}(z)\rangle = \Omega_{rest}$ at a fixed chemical potential μ, and Ω_{rest} is the grand potential for the restored phase.
We now turn to the accuracy of the Thomas-Fermi approximation in describing the grand potential for inhomogeneous phases. The comparison is performed exploiting the numerical values for the ν and Δ parameters of the modulation which are the results of the minimization of the exact grand potential Ω [16, 17]. These are inserted not only in Ω (for the respective chemical potential) but also in Ω_{TF_0}. We get the results reported in Fig 2.2

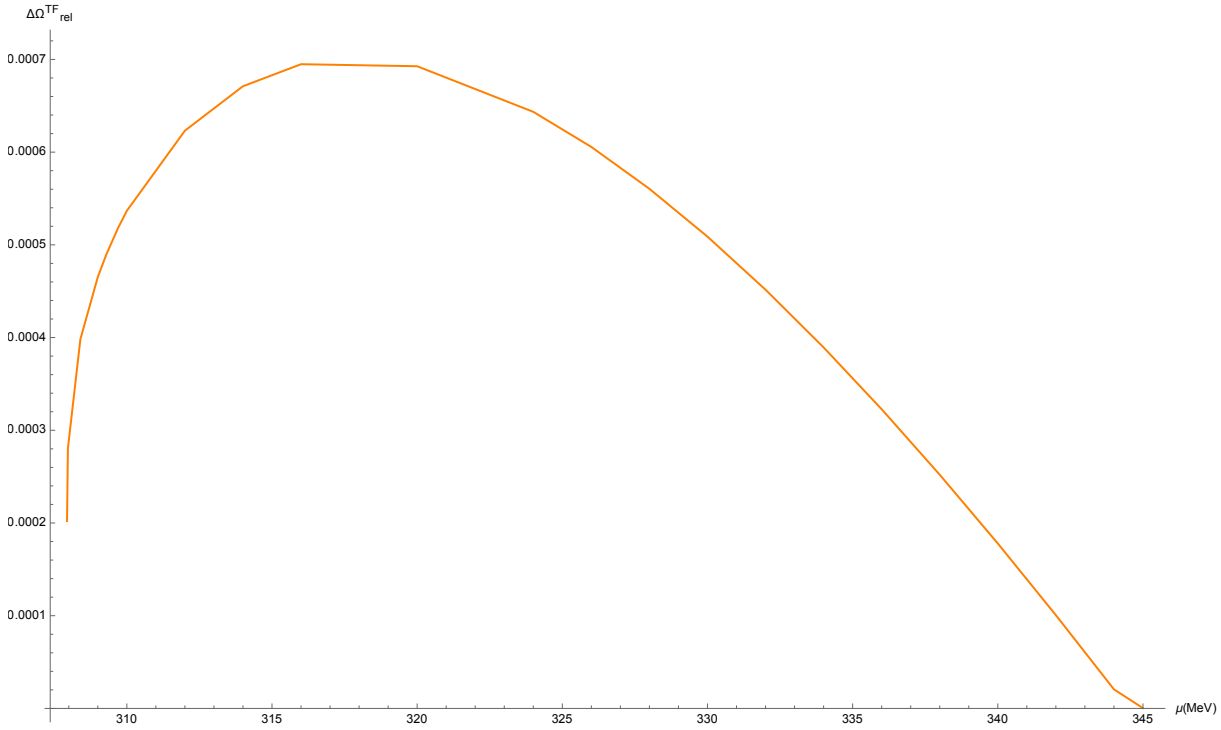

Figure 2.2: Relative error between Ω_{TF_0} and Ω. The values of the parameters are obtained through the numerical minimization of Ω.

Clearly, Ω_{TF_0} equals Ω in the homogeneous phase and is a good approximation for inhomogneoeus phases.

2.3 Improvement of the Thomas-Fermi approximation

When we make a comparison between homogeneous and inhomogeneous phases for chiral condensates, the differences are of the order of 0.01% [16, 17]. If we compare this order of magnitude with the relative error of the difference between our approximation and the numerical result, we see that we wouldn't be able to resolve the energetic differences between the restored and the inhomogeneous phases. Indeed, if we do not improve such approximation, the Thomas-Fermi method would be almost useless in the chemical potential window characteristic for inhomogeneous QCD phases in the core of Neutron Stars.
There is an important observation that needs to be taken into account with our first assumption on the Thomas-Fermi method. Assuming that the modulation was absent, we obtained the thermodynamic potential and subsequently we "added" a dependency of the condensate from the z coordinate. By doing this, we neglected all the non-diagonal elements that complicate enormously the problem of the diagonalization which depend on two different momenta in the Fourier representation of the hamiltonian matrix (see (2.19)). As a consequence, we expect that the terms that the Thomas-Fermi approach neglects are gradient terms, and we want now to add them to our approximation in order to improve it, obtaining a form for the grand potential that would be close to the numerical result for

inhomogeneous phases.
The method we would like to exploit is very simple: we consider the Thomas-Fermi approximation and we add the gradients of the solitonic modulation with respect to the space coordinate. We consider different fit functions (which, in general, depend on the chemical potential) multiplied to the gradients, in order to reproduce the exact result. We are actually forcing the gradients we are adding to improve the initial Thomas-Fermi approximation. Nevertheless, our scope in this chapter is to obtain an analitic approximation that will give us the possibility to consider the chiral, inhomogeneous condensate and, at the same time, the color superconductor (also inhomogeneous) in the 2SC phase. Indeed, without such approximation, it would be impossible analitically and numerically to consider both the condensates as spatially modulated.
In Chapter 4 instead, we will outline a mathematically rigorous procedure to obtain the approximate grand potential for the chiral condensate.

2.3.1 Gradients

Considering the solitonic modulation introduced in (2.34), the gradient terms we are going to add to our previous approximation are given by

$$|\nabla M(z,\Delta,\nu)| = \left|\Delta^2\nu cn(z\Delta|\nu) - \Delta^2\nu sn(z\Delta|\nu) + \frac{\Delta^2\nu^2 cn(z\Delta|\nu)^2 sn(z\Delta|\nu)^2}{dn(z\Delta|\nu)}\right| \tag{2.36}$$

Averaging over the period of the modulation we can introduce the quantities

$$A(\Delta,\nu) = \frac{1}{L[\Delta,\nu]}\int |\nabla M(z,\Delta,\nu)|^2 dz, \tag{2.37}$$

and

$$B(\Delta,\nu) = \frac{1}{L[\Delta,\nu]}\int |\nabla M(z,\Delta,\nu)|^4 dz. \tag{2.38}$$

2.3.2 First fit function

The first fit function we would like to use in order to reduce the difference between our approximation and the numerical result is given considering both the terms $A(\Delta,\nu)$ and $B(\Delta,\nu)$. The two fit functions (or the μ-dependent coefficients) will be such that

$$\Omega \approx \Omega_{TF_0} + c(\mu)A(\Delta,\nu) + d(\mu)B(\Delta,\nu), \tag{2.39}$$

where

$$c(\mu) = l_0 + l_1\frac{\mu}{\Lambda} + l_2\left(\frac{\mu}{\Lambda}\right)^2 + l_3\left(\frac{\mu}{\Lambda}\right)^3 \tag{2.40}$$

and

$$d(\mu) = d_0 + d_1\frac{\mu}{\Lambda} + d_2\left(\frac{\mu}{\Lambda}\right)^2 + d_3\left(\frac{\mu}{\Lambda}\right)^3 + d_4\left(\frac{\mu}{\Lambda}\right)^4. \tag{2.41}$$

For simplicity, we imposed $\Lambda = \Lambda_{PV}$.
In order to obtain such coefficients, we first consider $d(\mu) = 0$ and we take

$$\frac{\Omega(\Delta, \nu, \mu) - \Omega_{TF_0}(\Delta, \nu, \mu)}{A(\Delta, \nu)} = c(\mu), \tag{2.42}$$

obtaining

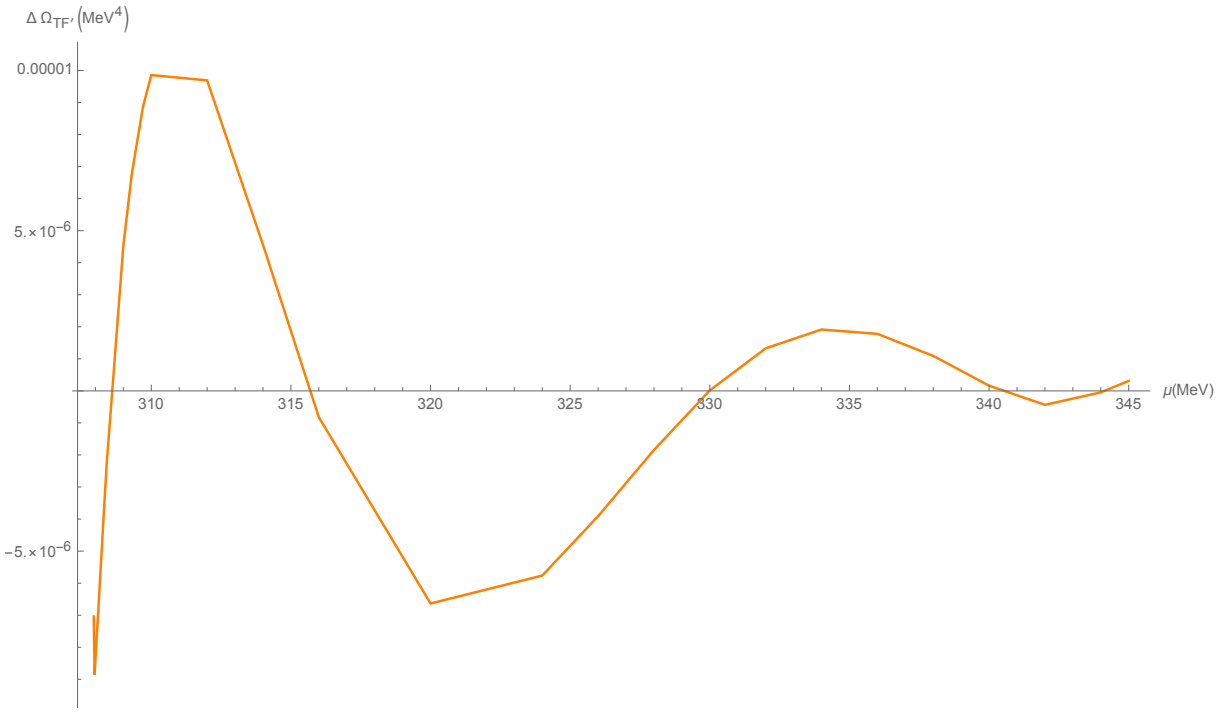

Figure 2.3: Relative error between $\Omega_{TF_0} + c(\mu)A(\Delta, \nu)$ and Ω. The values of the parameters Δ and ν are obtained through the numerical minimization of Ω.

We can see how the fit reduced of two orders of magnitude the difference between the Thomas-Fermi approximation and the exact result in the region that goes approximately from $\mu \approx 315$ MeV to $\mu \approx 345$ MeV.
Indeed, comparing the relative errors of the difference between the Thomas-Fermi approximation with and without the first gradient correction, we can see how it reduces from almost 0.07% at $\mu = 315$ MeV to an order of almost 0.0001%. Comparing the numerical values of the free energies, the difference between the Thomas-Fermi approximation and Ω is reduced from $\mathcal{O}(10^7)$ MeV^4 to $\mathcal{O}(10^5)$ MeV^4. Adding the second gradient in our expansion and proceeding similarly as before we get

$$\frac{\Omega(\Delta, \nu, \mu) - \Omega_{TF_0}(\Delta, \nu, \mu) - c(\mu)A(\Delta, \nu)}{B(\Delta, \nu)} = d(\mu) \tag{2.43}$$

and, as a consequence, the difference diminishes further

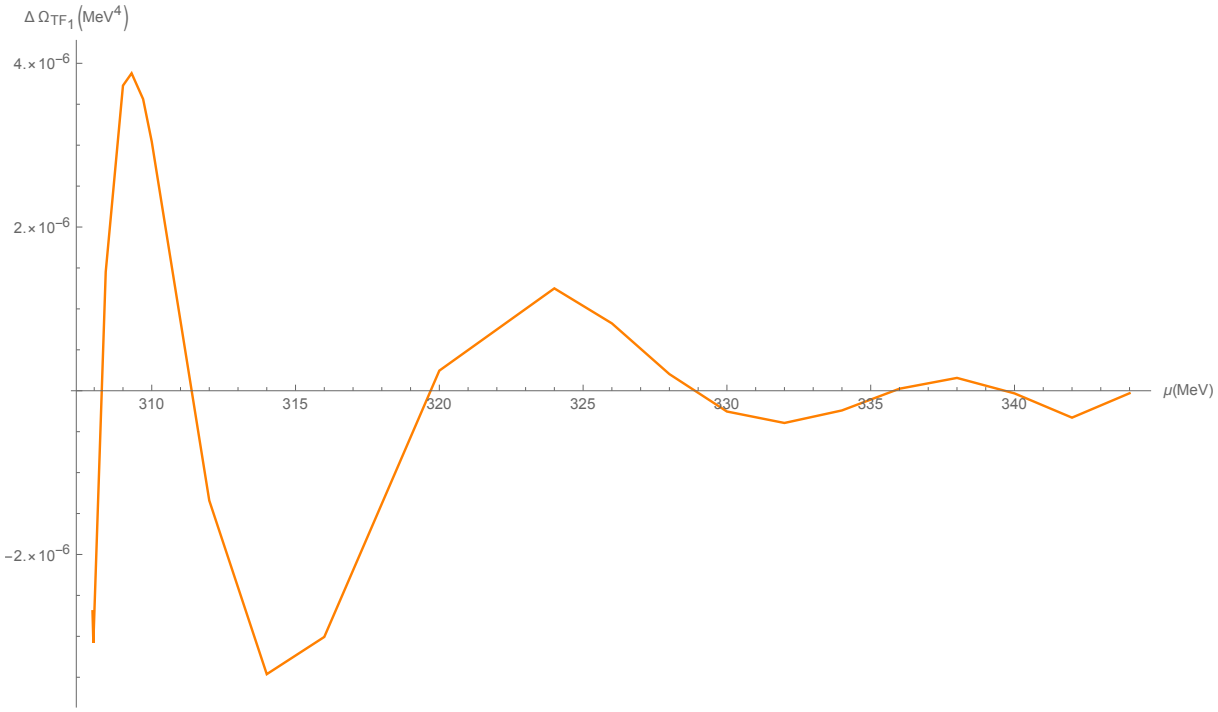

Figure 2.4: Relative error between $\Omega_{TF_1} = \Omega_{TF_0} + c(\mu)A(\Delta,\nu) + d(\mu)B(\Delta,\nu)$ and Ω. As before, the values of the Δ and ν parameters are obtained through the numerical minimization of Ω.

Therefore, forcing the gradients with this fit function, we see that the Thomas-Fermi approximation with this improvement could reach values which are significantly close to the exact result : for low chemical potentials, we have a relative error which is of the order of 0.0001%, reaching even a smaller percentage for higher values of the chemical potential. Considering the numerical values of the free energies, we find differences of $\mathcal{O}(10^5\ \text{MeV}^4)$, while at higher values of μ we reach of $\mathcal{O}(10^4\ \text{MeV}^4)$ - $\mathcal{O}(10^3\ \text{MeV}^4)$, which are sufficient for our qualitative results (considering that Ω has an order of magnitude of $\mathcal{O}(10^{10}\ \text{MeV}^4)$).

2.3.3 Second fit function

We consider a different fit function to find a way to consider only the square module of the gradients, rather than considering also the fourth-power terms. This could be relevant because we will have to perform a numerical minimization of the grand potential, which could be computationally demanding.
The attempt we are going to make involves a fit of the Δ parameter of the soliton solution as a function of the chemical potential, exploiting the numerical results obtained in [16, 17], thus considering

$$\Delta(\mu) = \Delta_0 + \Delta_1\mu + \Delta_2\mu^2 + \Delta_3\mu^3 + \Delta_4\mu^4. \tag{2.44}$$

Having obtained the expression of the Δ parameter of the soliton modulation, we can

introduce the coefficient

$$c_2\Big[\mu,\Delta(\mu)\Big] = h_0 + h_1\frac{\mu}{\Delta(\mu)} + h_2\Big(\frac{\mu}{\Delta(\mu)}\Big)^2 + h_3\Big(\frac{\mu}{\Delta(\mu)}\Big)^3 + h_4\Big(\frac{\mu}{\Delta(\mu)}\Big)^4 \tag{2.45}$$

to be added to the Ω_{TF_0} expression. As in the previous section, we consider the difference between Ω_{TF_0} and the full result in order to obtain the h_i numerical values of the $c_2\Big[\mu,\Delta(\mu)\Big]$ fit function. In this way, we find the difference plotted below

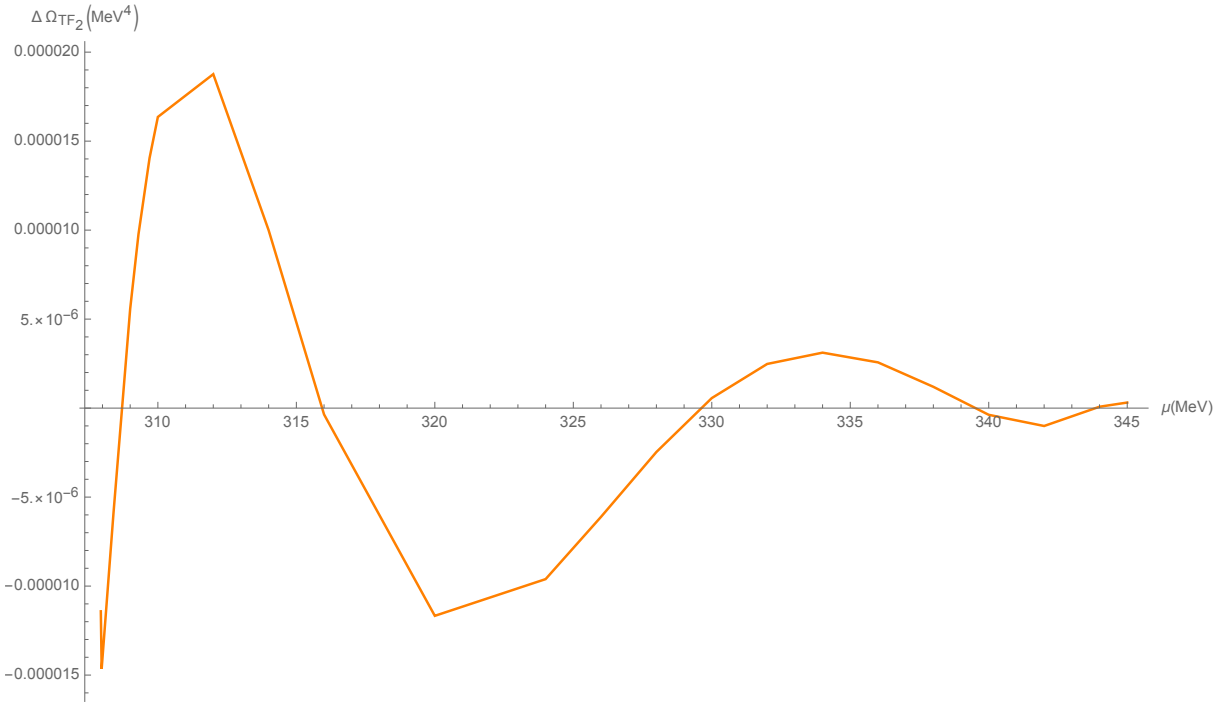

Figure 2.5: Relative error between $\Omega_2 = \Omega_{TF_0} + c_2(\mu)A(\Delta,\nu)$ and Ω. The values of the parameters Δ and ν are obtained through the numerical minimization of Ω.

In this case, we did not succeed in obtaining a gradient correction which is better than the first attempt. Nevertheless, also in this case, we can see from plot above that even in this case, we substantially reduced the difference between our approximation and the exact result.

2.3.4 Third fit function

The last μ-dependent coefficient for the gradient expansion that we would like to test is given by the introduction of an *effective* fit of the Δ parameter as a function of the ν parameter of the solitonic modulations at different values of μ

$$\Delta[\nu(\mu)] = s_0 + s_1\mu + s_2\mu^2 + s_3\mu^3 + s_4\mu^4, \tag{2.46}$$

which is represented in the following Figure

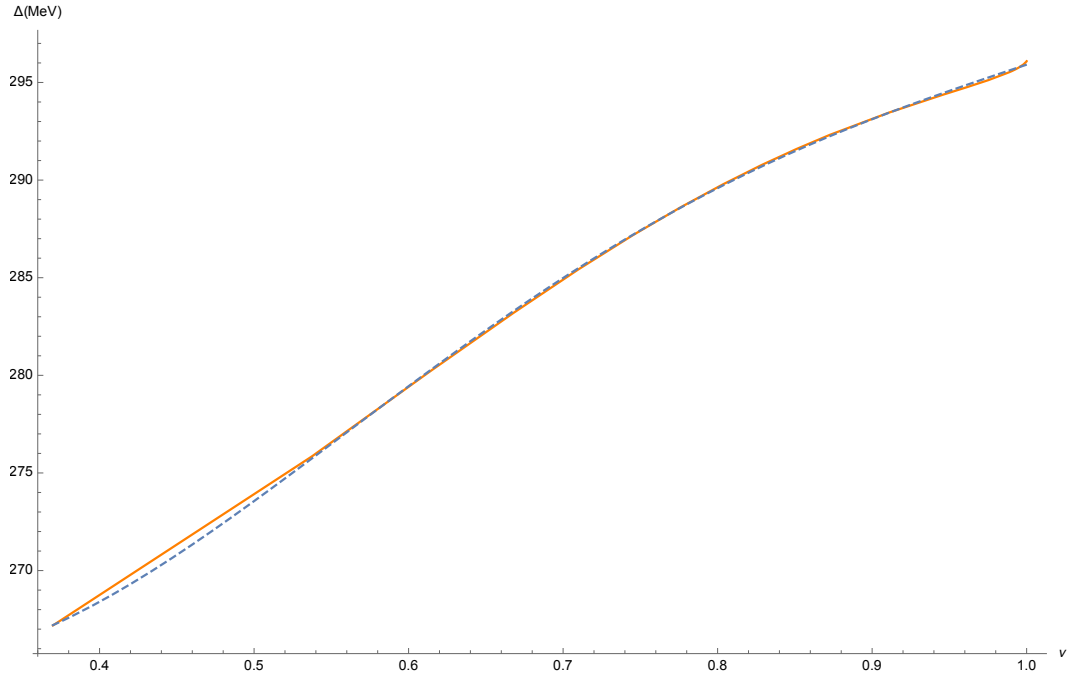

Figure 2.6: Effective fit for the Δ parameter as a function of the elliptic modulus ν.

This choice proved to be very efficient. Indeed, with this effective fit, we managed to have not only a very good approximation, but at the same time to include the minor possible number of terms in the gradient expansion of the Thomas-Fermi approximation, namely only the term $|\nabla M(z, \Delta, \nu)|^2$.
Having obtained the effective parameter $\Delta[\nu(\mu)]$ as a function of the chemical potential, we adopt the following expression for the coefficient of the squared module gradient term

$$c_3\Big[\mu, \Delta(\nu)\Big] = \sigma_0 + \sigma_1 \frac{\mu}{\Delta(\nu)} + \sigma_2 \Big(\frac{\mu}{\Delta(\nu)}\Big)^2 + \sigma_3 \Big(\frac{\mu}{\Delta(\nu)}\Big)^3 + \sigma_4 \Big(\frac{\mu}{\Delta(\nu)}\Big)^4. \tag{2.47}$$

Determining the σ_i coefficients as outlined for the other two fits and calling

$$\Omega_{TF_3}(\Delta, \nu, \mu) = \Omega_{TF_0}(\Delta, \nu, \mu) + c_3\Big[\mu, \Delta(\nu)\Big] A(\Delta, \nu), \tag{2.48}$$

the difference with the full result reduces to

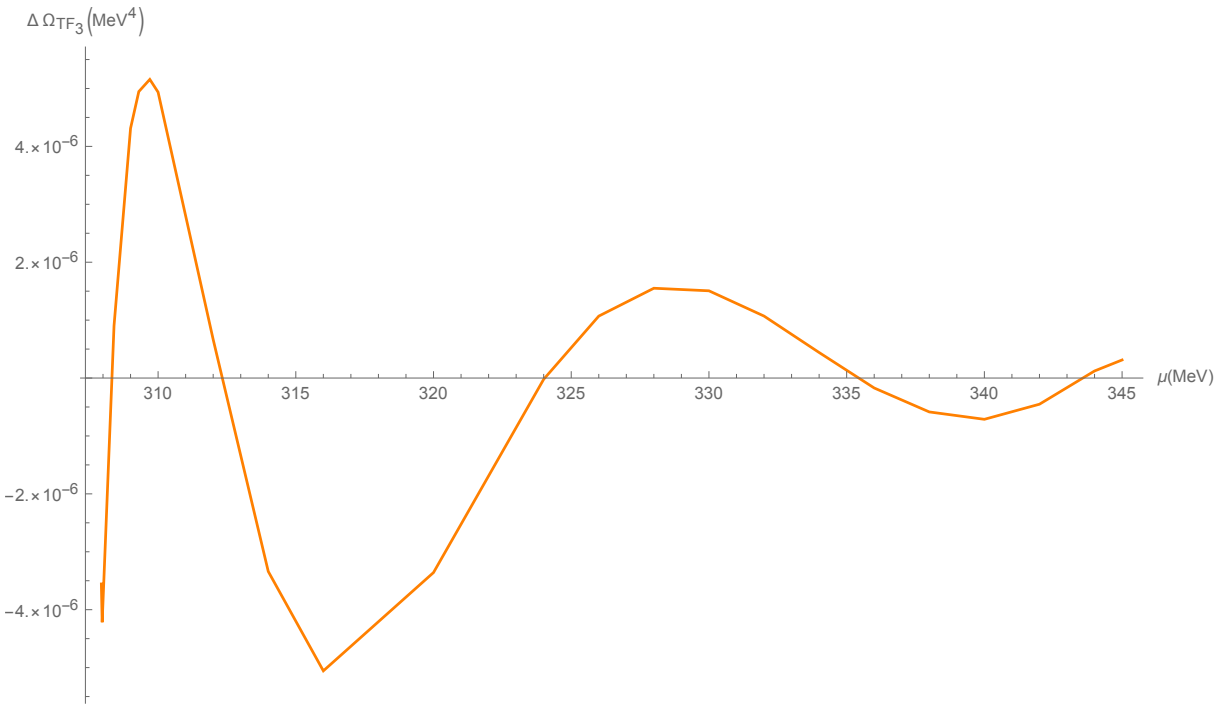

Figure 2.7: Relative error between the Ω_{TF_3} result and the numerical result Ω for different chemical potentials.

This fit function reduces the relative error of the difference between the Thomas-Fermi approximation and Ω to orders of 0.0001 %, which correspond an energetic difference form an order of $\mathcal{O}(10^5)$ MeV^4 and even $\mathcal{O}(10^4)$ MeV^4 for higher values of the chemical potential. In the following, given the simplicity of this expression, we will use this expression for the Thomas-Fermi improved approximation.

2.4 Improved Thomas-Fermi approximation

Despite we will use the values of the solitonic parameter derived from a numerical minimization of the hamiltonian matrix [16, 17], it is still interesting to plot the form of the grand potential that we approximated with the Thomas-Fermi. In this way, we can notice whether our expression exhibits the same minima for the same values of the parameters or not. In general, the Ω_{TF_3} expression will not have the same absolute minima as Ω; indeed, for high values of the chemical potential, there is a marked difference between the parameters that describe the minima of the approximated and of the numerical expression. It is natural, nevertheless, that such a difference exists and that it could be marked when looking at the values of the parameters. Indeed, when we improved our first Thomas-Fermi approximation, we forced the fit functions on the values of the parameters at different chemical potentials corresponding to the minima of Ω. This does not automatically induce the presence of a minimum for Ω_{TF_3}. What we have done with those fits was to force the approximation to resemble, in the best way possible, the exact result using the correct values of Δ and ν from previous works [16, 17]. We report in the following Figure the two

dimensional plot for the improved Thomas-Fermi form of the grand potential

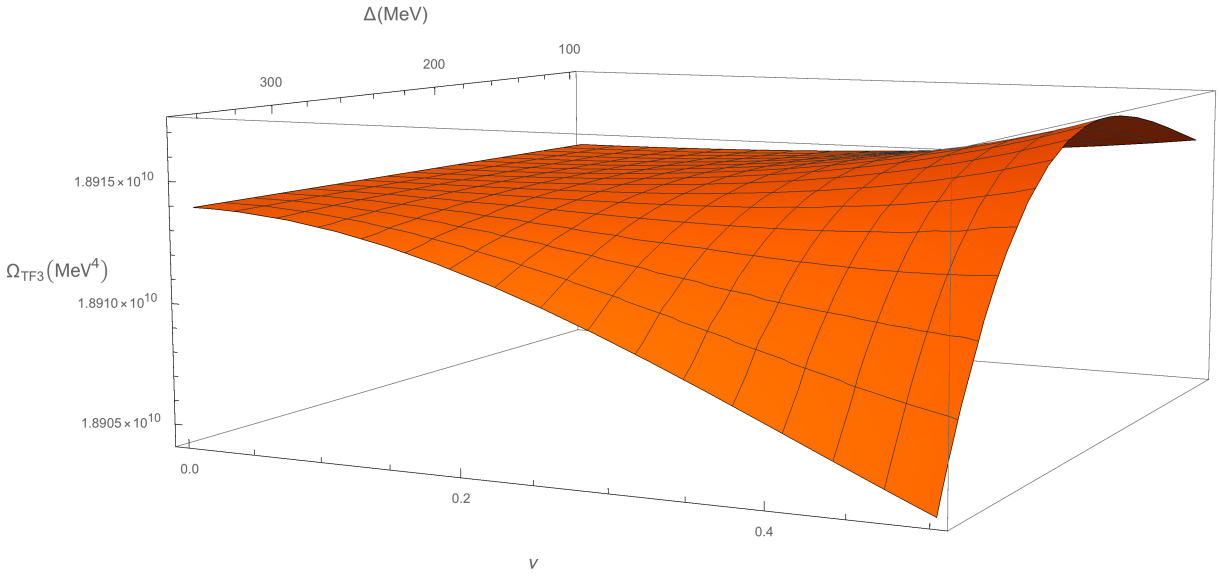

Figure 2.8: Plot of Ω_{TF_3} at $\mu = 340$ MeV.

For more clarity, we report the contour plot for Ω_{TF_3} at $\mu = 340$ MeV, where it is clear in which regions the minima of the thermodynamic potential are situated

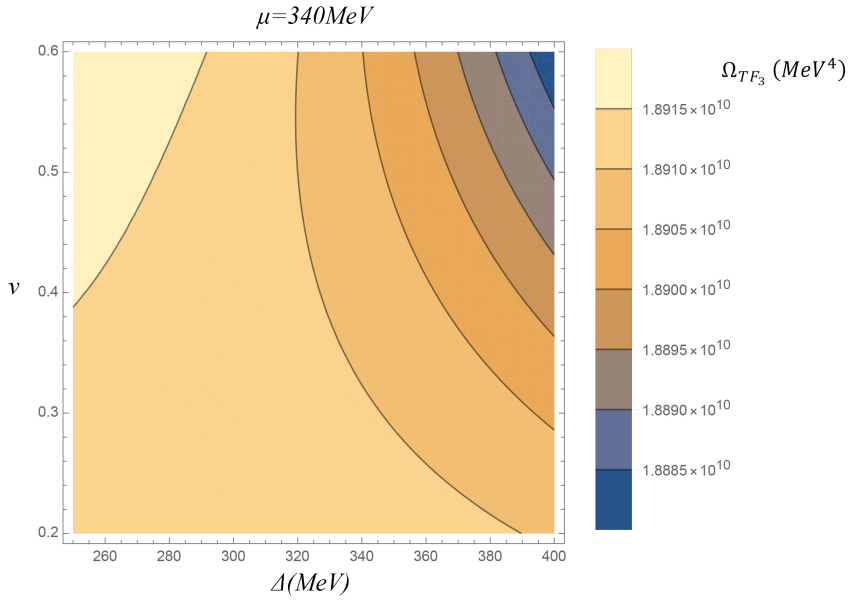

Figure 2.9: Contour plot of the thermodynamic potential with the improved Thomas-Fermi approximation at $\mu = 340$ MeV.

As shown in Figure 2.9, the region for the minimum value of the thermodynamic potential is restricted to a zone where the value of the Δ parameter is maintained on a value of 400 MeV while ν is approximately near the value of 0.6. If we compare, again, this values with the non-approximated problem, we get $\Delta = 280.222$ MeV and $\nu = 0.377$. Furthermore, as μ grows, the difference between the minima for the approximated and the numerical problem increases. Indeed, this tendency appears to be even more evident at $\mu = 344$ MeV, where for the Thomas-Fermi approximation we have $\nu \approx 0.6$ and $\Delta \approx 400$ MeV, while the exact results are $\nu = 0.136$ and $\Delta = 267.191$ MeV.
As explained before, it is natural to find such differences for the two grand potentials, as we are forcing the improved Thomas-Fermi result to follow Ω.

From now on, for simplicity, we will rename our preferred form for the Thomas-Fermi improved approximation $\Omega_{TF} = \Omega_{TF_3}$.

Chapter 3

Inhomogeneous color superconductivity and chiral condensate

As introduced in the first Chapter, color superconductivity is expected to be the favored state of deconfined quark matter at high values of the chemical potential. At asymptotic densities, it has been already proved by numerous authors [1, 2, 3] that the favored state is the CFL phase. Nevertheless, at lower baryonic densities, the CFL phase is expected to be no longer favored, and other paths of condensation could become favored.
In this work, we will consider the condensation pattern corresponding to the 2SC phase, where only two flavors of quark are involved (namely the *up* and *down* quarks). As shown for the chiral condensate, we will employ the NJL model to describe the interaction between quarks, substituting the gluon interaction with a point-like interaction. Furthermore, we will work, again, in the mean field approximation, neglecting fluctuations around the mean value for the condensate.
In the first Chapter, we introduced the non vanishing expectation value [1]

$$\langle q^T \mathcal{O} q \rangle, \tag{3.1}$$

where we specified that $\mathcal{O}$ is a total antisymmetric operator. Furthermore, we introduced the form for the color superconductor given by (1.9), which we recall for simplicity

$$z_{22} = \langle q^T i C \gamma_5 \tau_2 \lambda_2 q \rangle.$$

With this choice of the pairing pattern, blue up and down quarks do not condense and remain unpaired.
When considering both inhomogeneous chiral and 2SC condensates to be generated through a point-like interaction in the NJL model, the form of the Hamiltonian matrix is drastically complicated, and it is not possible to find a solution to the eigenvalue problem. We will briefly outline the procedure to obtain the Hamiltonian matrix involving both the homogeneous condensates and we will derive the expression for the grand potential in this case. After that, we will use the analytic improved Thomas-Fermi approximation to deal

with the chiral condensation and we will, eventually, perform a functional minimization in order to determine the inhomogeneous 2SC order parameter.

3.1 Eigenvalue problem for the chiral and the color superconductor condensates

The two flavor Lagrangian, involving only the degenerate lighter quarks ($m_{up} \approx m_{down}$), is given by [1, 17, 23]

$$\mathcal{L} = \mathcal{L}_{Dirac} + q^{\dagger}\mu q + \mathcal{L}_{chir} + \mathcal{L}_{2SC}, \tag{3.2}$$

where μ is the chemical potential and

$$\mathcal{L}_{Dirac} = \bar{q}(i\gamma^{\mu}\partial_{\mu} - \tilde{m})q. \tag{3.3}$$

The term in the Lagrangian which describes the chiral condensation pattern is, as before,

$$\mathcal{L}_{chir} = G[(\bar{q}q)^2 + (\bar{q}i\gamma^5\vec{\tau}q)^2], \tag{3.4}$$

while the Lagrangian for the color superconductor is given by

$$\mathcal{L}_{2SC} = G_D[(\bar{q}i\gamma_5 C\tau_2\lambda_2\bar{q}^T)(q^T Ci\gamma_5\tau_2\lambda_2 q)], \tag{3.5}$$

where G_D indicates the quark-quark coupling in the color-antitriplet channel, $C = i\gamma^2\gamma^0$ is the charge conjugation operator and τ_2 is the second Pauli matrix in flavor space. Adopting the mean field approximation, we can write the bilinear forms given by the diquark condensation pattern as

$$(\bar{q}q)^2 \approx \langle\bar{q}q\rangle(\bar{q}q) + (\bar{q}q)\langle\bar{q}q\rangle - \langle\bar{q}q\rangle\langle\bar{q}q\rangle \tag{3.6}$$

where we neglect the quadratic terms, which are the fluctuations around the expectation value. Expanding the full Lagrangian, we get

$$\begin{aligned}\mathcal{L} &= \bar{q}(i\gamma^{\mu}\partial_{\mu} - m)q + G\Big[2\langle\bar{q}q\rangle(\bar{q}q) - \langle\bar{q}q\rangle^2\Big] + \\ &+ G_D\Big[\langle q^T iC\gamma_5\tau_2\lambda_2 q\rangle^*(q^T iC\gamma_5\tau_2\lambda_2 q) - \langle q^T iC\gamma_5\tau_2\lambda_2 q\rangle(\bar{q}iC\gamma_5\tau_2\lambda_2\bar{q}^T) - |z_{22}|^2\Big]\end{aligned} \tag{3.7}$$

and so we can write

$$\begin{aligned}\mathcal{L} &= \bar{q}(i\gamma^{\mu}\partial_{\mu} - m + 2G\langle\bar{q}q\rangle)q - G\langle\bar{q}q\rangle^2 + \\ &+ G_D\Big[z_{22}^*(q^T iC\gamma_5\tau_2\lambda_2 q) - z_{22}(\bar{q}iC\gamma_5\tau_2\lambda_2\bar{q}^T) - |z_{22}|^2\Big] = \\ &= \bar{q}(i\gamma^{\mu}\partial_{\mu} - M)q + \frac{1}{2}\Big[\bar{q}SiC\gamma_5\tau_2\lambda_2\bar{q}^T - q^T iCS^*\gamma_5\tau_2\lambda_2 q - \frac{|S|^2}{2G_D}\Big] - \frac{|M-m|^2}{4G},\end{aligned} \tag{3.8}$$

where we identified the diquark gap as

$$S = -2G_D z_{22} \tag{3.9}$$

while, as in the case of the chiral condensation only, we defined an homogeneous effective mass given by

$$M = m - 2G\phi, \tag{3.10}$$

We introduce now the Nambu-Gorkov formalism, which is useful when considering color superconductivity for compactness, defining

$$Q = \frac{1}{\sqrt{2}} \begin{bmatrix} q \\ \\ q^C \end{bmatrix} \tag{3.11}$$

where $q^C = C\bar{q}^T$. The factor $1/\sqrt{2}$ needs to be taken into account because we are actually doubling the degrees of freedom of our problem, as we are considering q and q^C to be independent. In this way, the Lagrangian can be expressed in a more compact way

$$\mathcal{L} = \bar{Q} P^{-1} Q - \mathcal{V} \tag{3.12}$$

where with P^{-1} we indicated the inverse Nambu-Gorkov propagator, which is a 2×2 matrix in the Nambu-Gorkov space. Its explicit expression is given by

$$P^{-1} = \begin{bmatrix} i\gamma^\mu \partial_\mu - M + \mu\gamma^0 & S\gamma_5\tau_2\lambda_2 \\ \\ -S^*\gamma_5\tau_2\lambda_2 & -i\gamma^\mu\partial_\mu - M - \mu\gamma^0 \end{bmatrix}, \tag{3.13}$$

while the term in the Lagrangian containing the condensates contribution is given by

$$\mathcal{V} = \frac{|M-m|^2}{4G} + \frac{|S|^2}{4G_D}. \tag{3.14}$$

If we consider the condensates to be homogeneous in space, it is still possible to diagonalize the hamiltonian and to obtain the explicit expression for the eigenvalues of the quarks that participate to the coupling. Indeed, the explicit expression of the grand potential for the chiral and the 2SC color superconducting phases at zero temperature are given by [1, 23]

$$\Omega = -2N_f \int \frac{d^3p}{(2\pi)^3} \Big[E_b(\vec{p}) + E_S^+(\vec{p}) + E_S^-(\vec{p}) \Big] + \frac{|M-m|^2}{4G} + \frac{|S|^2}{4G_D} \tag{3.15}$$

where

$$E_b(\vec{p}) = \sqrt{p^2 + M_b^2} \tag{3.16}$$

for the blue quarks, while the eigenvalues for the quarks that are involved in the condensation pattern is given by

$$E^{\pm}_{red,green} = \sqrt{\left(\sqrt{p^2+M^2} \pm \mu\right)^2 + S^2} \equiv E^{\pm}_S(\vec{p}). \tag{3.17}$$

In this expression, the $\pm$ sign is for particles and antiparticles respectively. While, as mentioned before, $E^{\pm}_S(\vec{p})$ represent the two contributions for the quarks and antiquarks (respectively) involved in the 2SC pairing, the $E_b(\vec{p})$ eigenvalues correspond to the eigenenergies of the unpaired blue quarks that do not take place in the condensation pattern (indeed, the explicit expression of $E_b(\vec{p})$ does not include the S gap term for the 2SC condensate). The numeric coefficient is given by the fact that the total thermodynamic potential is expressed through the sum in flavor, color and spinor space (we have to consider the possible spins and the fact that we are considering particles and antiparticles). Furthermore, we have to add a factor 1/2, as we doubled the degree of freedom passing in the Nambu-Gorkov space.

3.2 Color superconductor as a perturbation

In this section, we outline the perturbative approach that we used in order to obtain the inhomogeneous 2SC color superconductor condensate. The problem is in general not analytically solvable, and we will exploit the approximation method developed in the previous Chapter for the chiral condensation pattern. We would like to underline that the results obtained in this section need to be considered on a qualitative level, due to the different assumptions that we will employ to tackle this problem. Indeed, there is not a general method to consider both the condensates spatially modulated even in 1D.
Furthermore, as stated previously, the approximation for the chiral condensate contribution to the grand potential has been obtained forcing the Thomas-Fermi functional form to reproduce the numerical result introducing a fit function for the gradient correction term. The task of outlining a rigorous derivation for an improved Thomas-Fermi approximation for the thermodynamic potential will be presented in the next Chapter.

If we assume that the order parameter describing the 2SC color superconductor is sufficiently small with respect to the chiral condensate, we can consider the quark-quark condensate as immersed in an inhomogeneous background given by the solitonic order parameter for the chirally broken phase. In this sense, we can rewrite the eigenvalues obtained in the previous section adopting a series expansion around a small S_0 value for the 2SC order parameter. The value of S_0 will be chosen arbitrarily (but in such a way to maintain the perturbative series under control), and in this work we will report the results of the numerical minimization for two different values of S_0 at two different orders of magnitude.

Keeping this in mind, we perform a series expansion centered in S_0 of (3.17) and write

$$E_S^{\pm}(\vec{p}) \approx \sqrt{\left(\sqrt{p^2+M^2} \pm \mu\right)^2 + S_0^2} + \frac{S_0(S-S_0)}{\sqrt{\left(\sqrt{p^2+M^2} \pm \mu\right)^2 + S_0^2}} + \frac{\left[\left(\sqrt{p^2+M^2} \pm \mu\right)^2\right](S-S_0)^2}{2\left(\left(\sqrt{p^2+M^2} \pm \mu\right)^2 + S_0^2\right)^{\frac{3}{2}}} + \mathcal{O}(S-S_0)^3. \tag{3.18}$$

Assuming that in the first term of the expansion $S_0 << M$, we can consider this term as a contribution to the thermodynamic potential given by the chiral condensate. So, if we consider the term deriving from $E_S^+(\vec{p})$, another one coming from $E_S^-(\vec{p})$ plus the one given by $E_b(\vec{p})$ and that in general the eigenvalues for the chiral, homogeneous phase for each quark color can be expressed as

$$E(\vec{p}) = \pm\sqrt{p^2+M^2} \pm \mu \tag{3.19}$$

for particles and antiparticles respectively, we can consider the total grand potential for both the inhomogeneous phases as

$$\Omega \approx \Omega_{chir} + \Delta\Omega_{2SC} \tag{3.20}$$

The next step is to consider the Ω_{chir} as the improved Thomas-Fermi approximation for the grand potential (in the form that we indicated as $\Omega_{TF_3} = \Omega_{TF}$ in the previous Chapter), while $\Delta\Omega_{2SC}$ is a perturbation due to the presence of a small, non-vanishing color superconducting order parameter.
Starting from the thermodynamic potential perturbative term for the 2SC condensate

$$\Delta\Omega_{2SC}(M, S_0, S) = -2N_f \int \frac{d^3p}{(2\pi)^3}\left[E_S^{*+}(\vec{p}) + E_S^{*-}(\vec{p})\right] + \frac{|S|^2}{4G_D} \tag{3.21}$$

where, adopting the above mentioned series expansion, we have that

$$E_S^{*+}(\vec{p}) \approx \frac{S_0(S-S_0)}{\sqrt{\left(\sqrt{p^2+M^2}+\mu\right)^2 + S_0^2}} + \frac{\left[\left(\sqrt{p^2+M^2}+\mu\right)^2\right](S-S_0)^2}{2\left(\left(\sqrt{p^2+M^2}+\mu\right)^2 + S_0^2\right)^{\frac{3}{2}}} + \mathcal{O}(S-S_0)^3 \tag{3.22}$$

and

$$E_S^{*-}(\vec{p}) \approx \frac{S_0(S-S_0)}{\sqrt{\left(\sqrt{p^2+M^2}-\mu\right)^2+S_0^2}} + \frac{\left[\left(\sqrt{p^2+M^2}-\mu\right)^2\right](S-S_0)^2}{2\left(\left(\sqrt{p^2+M^2}-\mu\right)^2+S_0^2\right)^{\frac{3}{2}}} + \mathcal{O}(S-S_0)^3. \tag{3.23}$$

We will present the results of the functional minimization limiting ourselves only to the first order term of the series expansions (3.22) and (3.23) (checking every time that the numerical results obtained for S are such that the terms $\mathcal{O}(S-S_0)^2$ and the higher orders are smaller than the leading term).
In our calculations, we will assume that the coupling G_D for the color superconductor is equal to $G/2$ (where G is the coupling for the quark-antiquark channel) [24].

If we consider a non-zero baryonic potential in (3.22) and (3.23), we do not have the possibility of getting an analytic expression for the integration over the quarks momenta: we need to perform the integral numerically and then we minimize with respect to the order parameter of the color superconductor condensate. The computational power required for the minimization is remarkable, as we perform the calculations adopting the Pauli-Villars regularization scheme. The choice of this regularization scheme is necessary, as we adopted this method for the determination of the free energy of the chiral condensate. For high values of μ and centering the series expansion in $S_0 = 0.01$ MeV, the results describe a very small amplitude with relevant fluctuations, and more computational power is required; instead, when we take $S_0 = 0.1$ MeV, we have the sufficient resolutive power to determine the shape of the 2SC order parameter. For now, we just want to point out that the procedure we outlined above for the functional minimization of the 2SC condensate as a perturbation is possible even including a nonzero chemical potential.
The results describe a 2SC modulation which has the same period of the chiral modulation, but there is a relative phase between the two, as the color superconductor has its minima where the chiral modulation has its maxima and vice versa. We succeeded in reproducing the expected behavior of the quark-antiquark condensate and the diquark one, but without the restriction of considering only one of them as spatially modulated. Indeed, we can say that we found the phase structure of the QCD diagram at intermediate and high baryonic density depicted in [8, 17], where there is a region of competition between the two condensates and, after the chiral symmetry restoration, an homogeneous 2SC gap S.
In addition to this, we obtained the results when both the condensates are inhomogeneous using the favored effective mass shape modulation for the chiral condensate.

3.2.1 Minimization with $S_0 = 0.01$ MeV and $S_0 = 0.1$ MeV

We can see from Fig 3.1 the results of the numerical minimization when $S_0 = 0.01$ MeV for $\mu = 310$ MeV

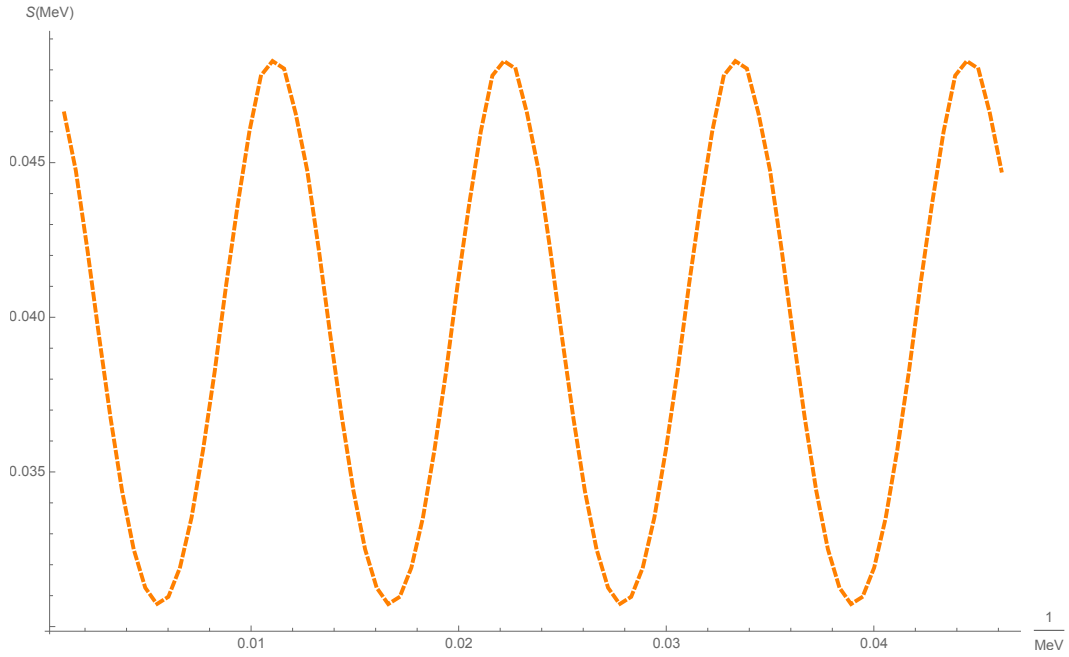

Figure 3.1: Results for the numerical minimization with respect to the order parameter for the color superconductor S, centering the series expansion for the eigenvalues at $S_0 = 0.01$ MeV when $\mu = 310$ MeV.

In Fig 3.1 we presented only the results for a low chemical potential; for higher values of the chemical potential and $S_0 = 0.01$ MeV, the resulting modulations exhibit serious fluctuations. Indeed, the amplitude is so small that more computational power is required to determine correctly the behavior of the S parameter as a result of the functional minimization.
Nevertheless, centering the series expansion at $S_0 = 0.1$ MeV, the amplitude of the the order parameter is greater, and we have sufficient computational power to resolve it clearly. Indeed, at $\mu = 310$ MeV and $S_0 = 0.1$ MeV, we obtained the results shown in Fig 3.2, while in Fig 3.3 we compare how the modulation changes when the chemical potential varies from $\mu = 310$ MeV to $\mu = 344$ MeV (close to the chiral restoration transition)

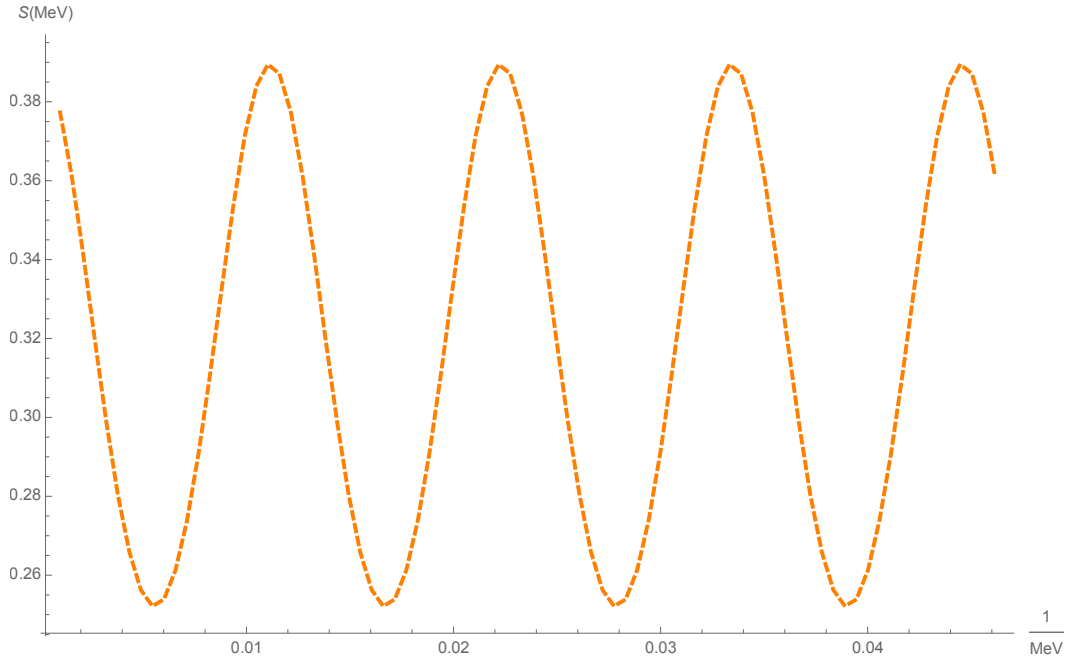

Figure 3.2: Results for the numerical minimization with respect to the order parameter for the color superconductor S, centering the series expansion for the eigenvalues at $S_0 = 0.1$ MeV when $\mu = 310$ MeV.

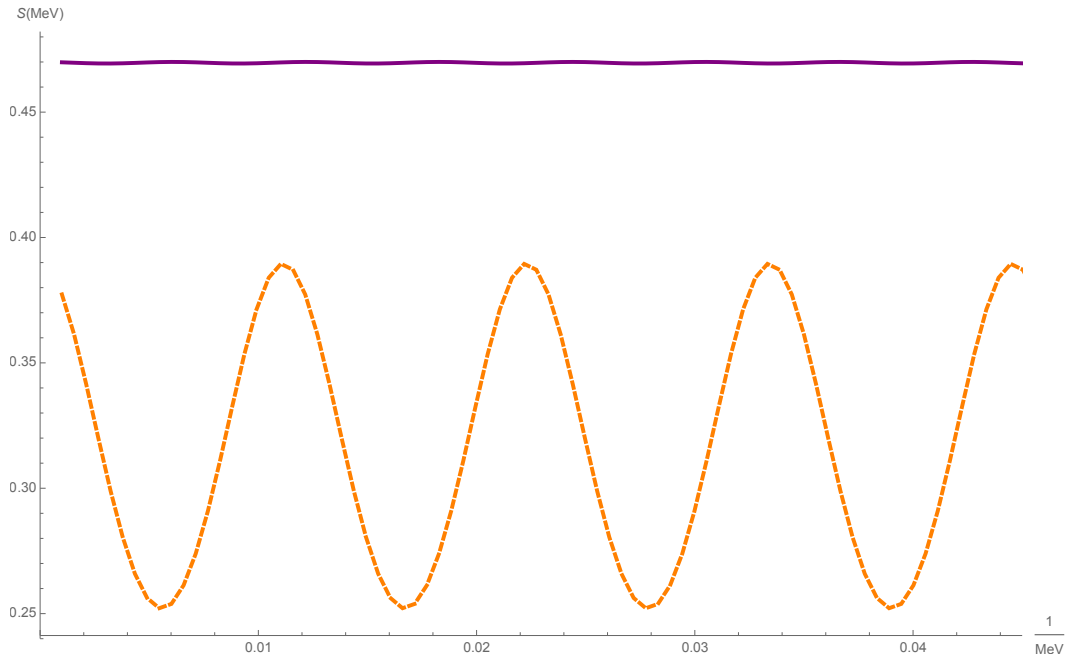

Figure 3.3: Results for the numerical minimization with respect to the order parameter for the color superconductor S, centering the series expansion for the eigenvalues at $S_0 = 0.1$ MeV when $\mu = 310$ MeV (orange, dashed line) and $\mu = 344$ MeV (purple, solid line).

We can see how the modulation is well defined for $\mu = 310$ MeV, while for increasing values of the chemical potential, the amplitude substantially reduces its value; this is not surprising, as the numerical minimization is performed using the set of values for the chiral condensate obtained from the numerical minimization of the thermodynamic potential when only this condensate is taken into consideration; indeed, for increasing values of μ, the chiral condensate vanishes ($M \to 0$). The corresponding value for the color superconductor is not null in this region of the chemical potential, as shown in [1, 8]: this represents the transition from the chirally broken phase to the restored one for the chiral condensate, while above $\mu = 345 - 350$ MeV the color superconductor is expected to be characterized by an homogeneous order parameter. In this way, we find (always on a qualitative level) the phase diagram determined in [8]; actually, through our calculations, we are able to overcome the first assumption made by the author, where, for the sake of finding an analytic result for the eigenvalues of the problem and to make the numerical minimization feasible, the 2SC condensate is assumed to be constant in space while the chiral condensate is described as a cosine modulation.

Chapter 4

Ginzburg-Landau expansion

In Chapter 2, we introduced a qualitative Thomas-Fermi approximation for chiral condensates whose shape is given by the 1D Jacobi elliptic functions, which, as we already said, are found to be the favored modulations at $T = 0$ and intermediate μ, namely the conditions expected in the core of Neutron Stars. Previously, we forced the thermodynamic potential to follow the exact result. Now we want to show that it is possible to obtain an approximation for the grand potential Ω in which the Thomas-Fermi term represents a series expansion with respect to one parameter of the condensate modulation (we will obtain such functional form for a plane wave modulation), while for the second parameter we find a gradient expansion a' la Ginzburg-Landau. We will show how such expansion is valid not only for every 1D shape, but even for higher dimensional modulations. This result is extremely important, because in this way we rigorously obtain an approximate thermodynamic potential that is valid in any region of the QCD phase diagram at T = 0. We will show, indeed, that not only we are able to reproduce with a very satisfying approximation the results for the chiral density wave solution of the eigenvalue problem and for the one dimensional solitonic modulation, but also the ones for 2D modulations.

4.1 Ginzburg-Landau gradient expansion

The Ginzburg-Landau theory of superconductivity gives an approximation for the thermodynamic potential when the order parameter related to the spontaneous symmetry breaking mechanism is small. Indeed, the expansion of the free energy of the system is possible only in proximity of a second order phase transition, and in particular in the neighborhood of critical points. Actually, not only the condensate must be small, but also its gradients.
Initially, the Ginzburg-Landau theory was conceived for ordinary superconductivity, but it has been extensively adopted in case of quark deconfinement in presence of chiral and color superconducting condensates [1, 3, 5, 16, 17].
We can adapt the Ginzburg-Landau expansion to the NJL model in the mean field approximation, through which we assume that the condensate is represented by its mean value neglecting fluctuations. In this context, always working in the chiral limit, and assuming as before that the pseudoscalar contribution to the effective mass is pointing in the third direction

$$\phi_p^i = \delta_{i,3}\phi_p^3,$$

we can write the explicit expression for the grand potential

$$\Omega_{MF}(M) = \Omega_{MF}(0) + \frac{1}{V}\int dV\Big[\frac{1}{2}\alpha_2|M(\vec{x})|^2 + \frac{1}{4}(\alpha_{4,a}|M(\vec{x})|^4 + \alpha_{4,b}|\nabla M(\vec{x})|^2) + ...\Big]. \quad (4.1)$$

The coefficients α that appear inside the expansion, multiplied for the effective mass and its gradients terms, are functions of the chemical potential and the temperature, and they do not depend on the particular expression of the condensate. Through their dependence from T and μ, they determine the structure in the phase diagram for the effective mass. The convention for the α coefficients is to label them with a number corresponding to the total power with which the parameters of the modulation appear in the expansion.
Analyzing the signs of these coefficients, we can get an insight on the behavior of the condensate and even define the position of phase transition regions in the phase diagram. For example, when the $\alpha_{4,b}$ coefficient is positive, we find the homogeneous phase, as the gradient terms in the expansion are disfavored [17]. When $\alpha_{4,a} > 0$ and $\alpha_2 < 0$, the favored solution has a nonzero mass given by

$$|M| \simeq \sqrt{-\frac{\alpha_2}{\alpha_{4,a}}} \quad (4.2)$$

while $|M| = 0$ if $\alpha_2 > 0$. A phase transition occurs at $\alpha_2 = 0$ from the homogeneous chiral broken phase to the restored phase. Indeed, we can trace in the phase diagram a transition line. The onset for inhomogeneous phases is signaled by a negative sign for the $\alpha_{4,b}$ coefficient.
Through this brief introduction to this method, we showed how powerful the Ginzburg-Landau expansion is, but actually we must keep in mind that this is possible only when the order parameter, close to a second order phase transition, is small.

4.2 Improved Ginzburg-Landau expansion

We now present a rigorous derivation of an expansion for the free energy of dense, deconfined quark matter through which we are able to characterize the thermodynamic properties of such system in every region of the QCD phase diagram at T = 0. We will show how this method, which we will define *improved Ginzburg-Landau* (IGL) method, can successfully reproduce the grand potential for inhomogeneous chiral condensates in one or higher dimensions. We will begin considering a simple plane wave modulation for the derivation of Ω_{IGL} and we will generalize the results for arbitrary periodic structures, presenting in the following sections a comparison between our results and the ones obtained for the solutions of the eigenvalue problem obtained through the numerical diagonalization of the hamiltonian matrix.
Let us consider the 1D modulation

$$M(z) = \Delta e^{2iqz}, \quad (4.3)$$

which is called *chiral density wave* (CDW), and suppose to consider a region of the QCD phase diagram at high chemical potential and zero temperature, where the modulation is characterized by a small Δ amplitude. When we work in the neighborhood of a transition line, the Ginzburg-Landau theory suggests that we can approximate the grand potential through a gradient expansion for both the parameters that characterize the condensate.
If we begin expanding the thermodynamic potential with respect to the Δ parameter, we would get an expression of the form

$$\Omega = \Omega_0 + \Omega_2(q)\Delta^2 + \Omega_4(q)\Delta^4 + ... \tag{4.4}$$

where, in principle, $\Omega_2(q)$ and $\Omega_4(q)$ could be arbitrary functions of the q parameter.
Expanding also in the second parameter q, we would get an expression of the form

$$\Omega = \Omega_0 + c_{20}\Delta^2 + c_{22}\Delta^2 q^2 + c_{24}\Delta^2 q^4 + ... + c_{40}\Delta^4 + c_{42}\Delta^4 q^2 + ..., \tag{4.5}$$

where the coefficients c_{ij} have the first index corresponding to the power of Δ, while the second to the q parameter.
We want to show that $\Omega_0 = \Omega_{rest}$ (which is the grand potential of the restored phase) and we will write all the terms that do not depend on q as the Thomas-Fermi approximation $\Omega_{TF}(\Delta)$ (that is given by the functional form of the thermodynamic potential for an homogeneous effective mass, where we substitute the homogeneous order parameter M with the spatial average of $M(z)$). In this way

$$\Omega_{TF}(\Delta) \simeq \Omega_0 + \sum_i c_{i0}\Delta^i. \tag{4.6}$$

We start considering the series expansion (4.4), assuming a condensate whose shape is represented by (4.3).
The CDW modulation eigenvalues could be found analitically [16, 17, 20], and they are given by

$$\lambda_\pm = \sqrt{p_z^2 + \Delta^2 + \pm 2q\sqrt{p_z^2 + \Delta^2}}. \tag{4.7}$$

Using the boosting method, introduced in Chapter 2, we can obtain the 3D eigenvalues from the one-dimensional $\lambda_\pm$, which are given by

$$E_\pm = \sqrt{p_\perp^2 + \lambda_\pm^2}. \tag{4.8}$$

Using the Pauli-Villars regularization scheme we can write, at $T = 0$,

$$\begin{aligned} \Omega &= -\frac{N_c N_f}{4\pi^2}\int_0^\infty dp_\perp p_\perp \int_{-\infty}^\infty dp_z \sum_{\sigma=\pm}\left[E_{PV}^\sigma + (\mu - E^\sigma)\theta(\mu - E^\sigma)\right] = \\ &= -\frac{N_c N_f}{4\pi^2}\int_0^\infty dp_\perp p_\perp \int_{-\infty}^\infty dp_z \sum_{\sigma=\pm}\omega_\sigma. \end{aligned} \tag{4.9}$$

Now we would like to write an expansion, following the expression (4.4), in such a way that

$$\Omega = \Omega_0 + \frac{\partial\Omega}{\partial(\Delta^2)}\Big|_{\Delta=0}\Delta^2 + \frac{1}{2}\frac{\partial^2\Omega}{\partial(\Delta^2)^2}\Big|_{\Delta=0}\Delta^4 + ... \tag{4.10}$$

identifying the different terms with

$$\Omega_{rest} = \Omega_0, \qquad \Omega_2(q) = \frac{\partial\Omega}{\partial(\Delta^2)}\Big|_{\Delta=0}, \qquad \Omega_4(q) = \frac{1}{2}\frac{\partial^2\Omega}{\partial(\Delta^2)^2}\Big|_{\Delta=0}. \tag{4.11}$$

Starting from the Ω_0 term, we can integrate separately the vacuum and the medium contribution (that we have already isolated in (4.9)). Referring to the results presented in the Appendix A, we can obtain the analytic expression for the vacuum contribution of Ω_0 obtaining

$$\Omega_0^{vac} = \frac{3}{4}\frac{N_c N_f}{4\pi^2}\Lambda^4 \log[\frac{27}{16}] \tag{4.12}$$

and for the medium contribution instead

$$\Omega_0^{med} = -\frac{N_c N_f}{12\pi^2}\mu^4, \tag{4.13}$$

which are independent of q, as they should. In this way, we verified that actually Ω_0 corresponds to Ω_{rest}.
Now we focus on the second term of the (4.11) expansion. The full, explicit computation is developed in Appendix A. We have

$$\Omega_2(q) = \frac{\partial\Omega}{\partial(\Delta^2)}\Big|_{\Delta=0} = -\frac{N_c N_f}{4\pi^2}\int_0^\infty dp_\perp p_\perp \int_{-\infty}^{\infty} dp_z \sum_{\sigma=\pm}\frac{\partial\omega_\sigma}{\partial(\Delta^2)}. \tag{4.14}$$

Separating the different contributions that come from the vacuum and medium terms we have

$$\begin{aligned}
\Omega_{2,1}^{vac} &= -3\frac{N_c N_f}{8\pi^2}\Lambda^2 \log\left(\frac{4}{3}\right), \\
\Omega_{2,2}^{vac} &= -q\frac{N_c N_f}{4\pi^2}\sum_k c_k\Big[(q-\sqrt{q^2+k\Lambda^2})\log(k\Lambda^2) + 2\sqrt{q^2+k\Lambda^2}\log(q+\sqrt{q^2+k\Lambda^2})\Big],
\end{aligned} \tag{4.15}$$

for the vacuum terms while for the medium part we get

$$\begin{aligned}
\Omega_{2,1}^{med} &= \frac{N_c N_f}{4\pi^2}\mu^2, \\
\Omega_{2,2}^{med} &= q\frac{N_c N_f}{4\pi^2}\Big[(\mu-q)\log\left(\frac{|\mu-q|}{q}\right) - (\mu+q)\log\left(\frac{|\mu+q|}{q}\right)\Big].
\end{aligned} \tag{4.16}$$

Now, if we expand the terms of Ω_2 that depend on q for small values of this parameter, we find the Ginzburg-Landau coefficients. Indeed, expanding $\Omega_{2,2}^{vac}$ and $\Omega_{2,2}^{med}$

$$\begin{aligned}\Omega_{2,2}^{vac}+\Omega_{2,2}^{med}=\frac{N_cN_f}{4\pi^2}\Big\{\Lambda^2\Big[(2-\log(\frac{32}{3})+\log(\frac{\Lambda^2}{q^2}))\frac{q^2}{\Lambda^2}+\frac{11q^4}{9\Lambda^4}-\frac{17q^6}{27\Lambda^6}+...\Big]+\\+\mu^2\Big[-(2+\log(\frac{\mu^2}{q^2}))\frac{q^2}{\mu^2}+\frac{q^4}{3\mu^4}+\frac{q^6}{10\mu^6}+...\Big]\Big\}\end{aligned} \tag{4.17}$$

and simplifying the above expression, we get

$$\begin{aligned}\Omega_{2,2}^{vac}+\Omega_{2,2}^{med}=\frac{N_cN_f}{4\pi^2}\Big[-\log\Big(\frac{32\mu^2}{3\Lambda^2}\Big)q^2+\frac{1}{3}\Big(\frac{11}{3\Lambda^2}+\frac{1}{\mu^2}\Big)q^4+\\+\Big(\frac{1}{10\mu^4}-\frac{17}{27\Lambda^4}\Big)q^6+\Big(\frac{230}{567\Lambda^6}+\frac{1}{21\mu^6}\Big)q^8+...\Big].\end{aligned} \tag{4.18}$$

If we recall the series expansion introduced in eq.(4.5), we have that we can group all the terms that do not depend on the wavevector q inside the Thomas-Fermi expression for the grand potential (eq. (4.6)), while $\Omega_2(q)$ contains all the terms of the form $c_{22}q^2+c_{24}q^4+c_{26}q^6+...$ If we look at the CDW modulation (4.3), we see that we can write all the terms that appear with even powers of the q parameter as a gradient expansion in terms of the plane wave modulation, in such a way that

$$\Omega\simeq\Omega_{TF}(\Delta)+\alpha_4(\mu)|\nabla M|^2+\alpha_6(\mu)\Big(3|M|^2|\nabla M|^2+\frac{1}{2}|\nabla^2M|^2\Big)+\alpha_8(\mu)|\nabla^3M|^2+\alpha_{10}(\mu)|\nabla^4M|^2 \tag{4.19}$$

where we adopted the convention of labeling the Ginzburg-Landau coefficients with indices that indicate the total power of the product of the parameters that describe the modulation of the chiral condensate. We truncated the gradient expansion at the total power of ten, as it will suffice for our purposes. In eq. (4.19) we added the $|M|^2|\nabla M|^2$ term, which comes from the $c_{42}\Delta^4q^2$ contribution in eq. (4.5), as it has the same power of $|\nabla^2M|^2$.
The explicit expressions of Ginzburg-Landau coefficients are

$$\begin{aligned}\alpha_4(\mu)&=-\frac{N_cN_f}{16\pi^2}\log\Big(\frac{32\mu^2}{3\Lambda^2}\Big),\\ \alpha_6(\mu)&=\frac{N_cN_f}{96\pi^2}\Big(\frac{11}{3\Lambda^2}+\frac{1}{\mu^2}\Big),\\ \alpha_8(\mu)&=\frac{N_cN_f}{256\pi^2}\Big(\frac{1}{10\mu^4}-\frac{17}{27\Lambda^4}\Big),\\ \alpha_{10}(\mu)&=\frac{N_cN_f}{1024\pi^2}\Big(\frac{230}{567\Lambda^6}+\frac{1}{21\mu^6}\Big).\end{aligned} \tag{4.20}$$

We would like to underline as the present expansion, given in terms of the Thomas-Fermi term plus the Ginzburg-Landau-like gradient expansion, does not depend on the specific modulation we are considering (or its dimensionality), as the coefficients depend only on the chemical potential. More precisely, they depend on both μ and Λ. The dependence on the regularization scale is due to the fact that the underlying theory is the NJL model regularized with the Pauli-Villars regularization scheme.
The above calculations have been performed considering a plane wave, but we can generalize such results to all the periodic modulations, rewriting the expansion as

$$\begin{aligned}\Omega \simeq \Omega_{TF}(\sqrt{\langle|M(z)|^2\rangle}) + \alpha_4(\mu)|\nabla M|^2 + \alpha_6(\mu)\Big(3|M|^2|\nabla M|^2 + \frac{1}{2}|\nabla^2 M|^2\Big) + \\ + \alpha_8(\mu)|\nabla^3 M|^2 + \alpha_{10}(\mu)|\nabla^4 M|^2.\end{aligned} \tag{4.21}$$

In the above expression, we substituted the argument of the Thomas-Fermi term with $\sqrt{\langle|M(z)|^2\rangle}$. Indeed, when we consider the $\Omega_{TF}(\sqrt{\langle|M(z)|^2\rangle})$ contribution, we have to perform a spatial average above the modulation period. This simply reduces to $\sqrt{\langle|M(z)|^2\rangle} = \Delta$ for a CDW, but in general the expression could be much more complicated for other modulations. Furthermore, with the above notation, we indicate that the gradient terms too need to be spatially averaged

$$|\nabla M|^2 \equiv \langle|\nabla M|^2\rangle\,. \tag{4.22}$$

This is unessential for a plane wave modulation as the CDW appears with its modulus, but this definition matters when we will consider more complicated modulations.
In the next section, we will illustrate how this approximation is actually a powerful tool to handle not only of 1D modulation, but also 2D crystalline structures.

4.3 CDW with the improved Ginzburg-Landau expansion

When we consider a chiral density wave (that we write again for simplicity)

$$M(z) = \Delta e^{2iqz} \tag{4.23}$$

in the improved Ginzburg-Landau approximation, we get an expression as

$$\begin{aligned}\Omega \simeq \Omega_{TF}(\sqrt{\langle|M(z)|^2\rangle} = \Delta) + 4\alpha_4 q^2\Delta^2 + \alpha_6\Big(12\Delta^4 q^2 + 8q^4\Delta^2\Big) + \\ + 64\alpha_8 q^6\Delta^2 + 256\alpha_{10}q^8\Delta^2.\end{aligned} \tag{4.24}$$

We can determine through a numerical minimization at different chemical potentials the values of the parameters Δ and q. Furthermore, we can actually compare our results with the ones found in [16, 17], where the numerical computation is presented. For the Δ parameter of the modulation we obtain the results reported in Fig 4.1

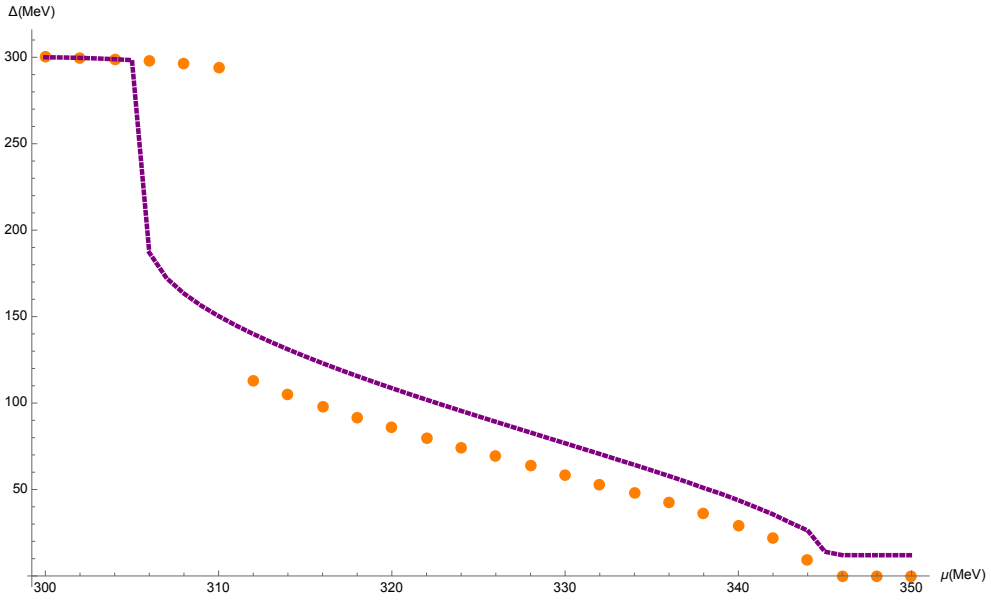

Figure 4.1: Comparison between the values of Δ obtained through the minimization of the free energy as a function of the chemical potential μ with two different methods. The dotted line (orange) corresponds to the numerical values, while the dashed line (purple) is obtained minimizing the improved Ginzburg-Landau grand potential eq.(4.24).

while for the wavevector q we have

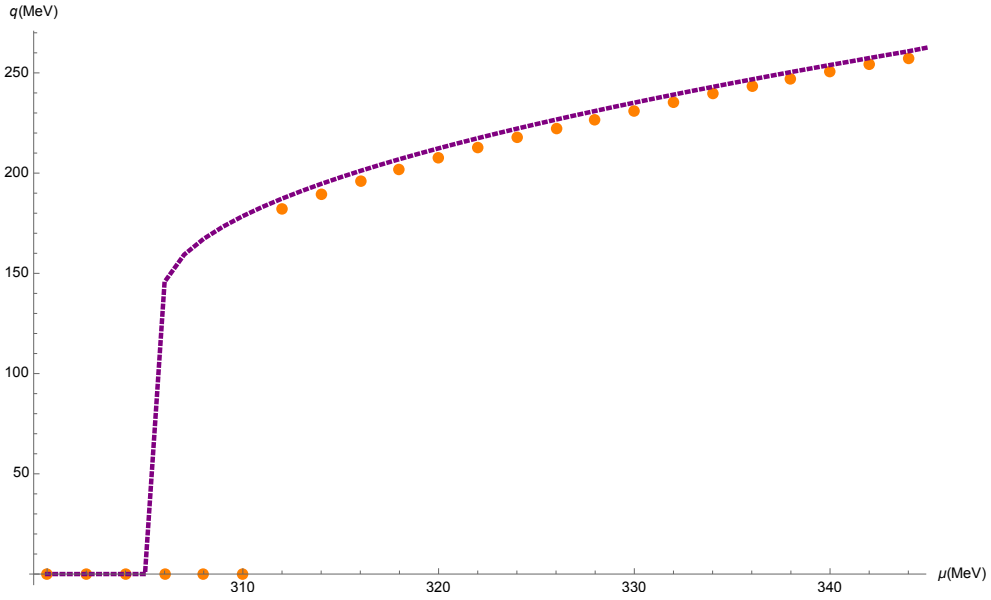

Figure 4.2: Values of q obtained through the minimization of the free energy as a function of the chemical potential μ with two different methods. The dotted line (orange) corresponds to the numerical values while the dashed line (purple) is obtained minimizing eq.(4.24).

We can see how the two parameters that minimize the thermodynamic potential are well reproduced by our approximation. There is a difference of almost 3-4 MeV for the

onset of the inhomogeneous phase with respect to the numerical computation (signaled by a discontinuity in both the parameters, as it happens through a first order phase transition). Indeed, in our approximation, we find that this happens at $306 - 307$ MeV, while from the numerical results we find that this occurs at 310 MeV: before this threshold, the q parameter that minimizes Ω^{CDW} has a null value, meaning that the order parameter is homogeneous.
However, we can argue that this difference is not substantial, and that in general the values of the parameter determined with the IGL expansion are greater than the ones determined from the numerical computation (we will show that this is true not only for the chiral density wave, but also for the solitonic solutions and in general also for higher dimensional crystalline structures). With a good approximation level, we can actually predict the occurrence of inhomogeneous phases in the QCD phase diagram, remembering that there is an error of the order of the MeV when adopting the improved Ginzburg-Landau method for the thermodynamic potential.
Plotting in Fig 4.3 the difference between the full thermodynamic potential for the CDW modulation Ω^{CDW} and Ω_{rest} compared with our IGL grand potential minus Ω_{rest}, we can see how we are able to reproduce with a very good approximation the energetic difference between inhomogeneous and the chiral restored phase

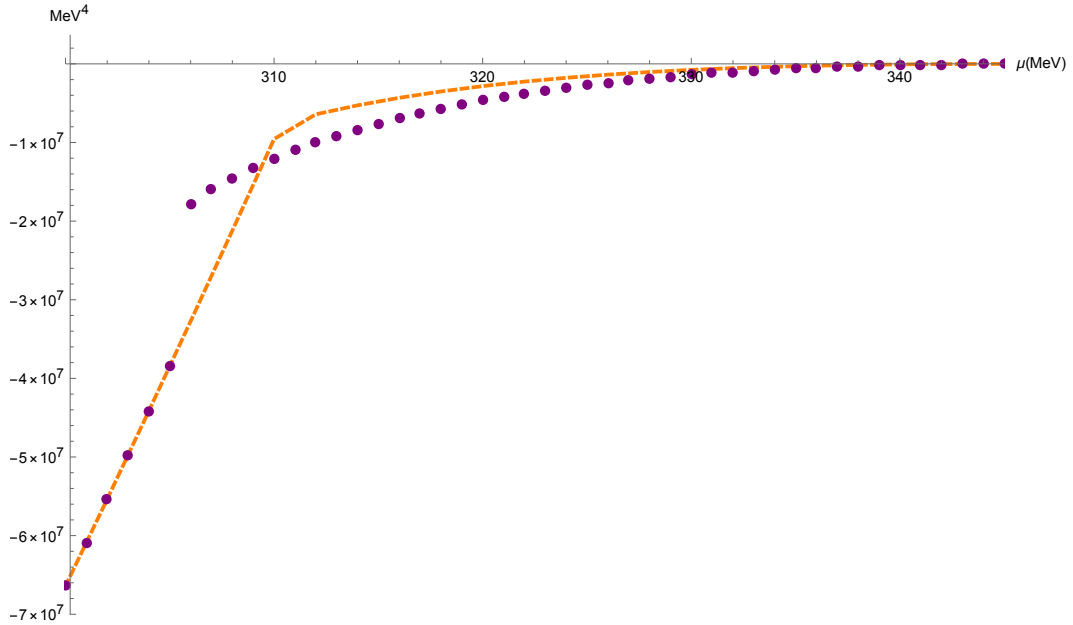

Figure 4.3: Plot of the difference between Ω^{CDW}_{IGL} and the thermodynamic potential for the restored phase as a function of μ (purple, dotted line); in orange (dashed), difference between the numerical result for Ω^{CDW} and Ω_{rest} for different values of the chemical potential.

As we have already outlined before, there is a slight difference between the prediction of the value of the chemical potential at which the onset for the inhomogeneous takes place. Nevertheless, we can see how our approximation is able to describe the thermodynamic properties of the inhomogeneous chiral density wave: we are allowed to determine whether

inhomogeneous phases are energetically more favored with respect to the restored phase. In the next section we will prove with similar numerical results that we can obtain even better predictions for the thermodynamic potential in the case of the 1D soliton solution, which are found to be the favored one-dimensional modulations.

4.4 1D solitonic solution with improved Thomas-Fermi expansion

We will now present the results for the 1D soliton solutions. We recall that the modulation is given by

$$M(z) = \Delta\nu \frac{sn(\Delta z|\nu)cn(\Delta z|\nu)}{dn(\Delta z|\nu)}, \tag{4.25}$$

where sn, cn and dn are respectively the elliptic sine, the elliptic cosine and the delta amplitude and whose period is given by

$$L(\Delta, \nu) = 2\frac{\mathcal{K}(\nu)}{\Delta} \tag{4.26}$$

where $\mathcal{K}(\nu)$ is a complete elliptic integral of first kind and $\nu \in [0,1]$ is the elliptic modulus. We now report the results for the numerical minimization of the parameters that characterize the solitonic modulation for each value of μ in the inhomogeneous window for QCD phases in high baryonic density environments. For the Δ parameter we obtain the results shown in Fig 4.4

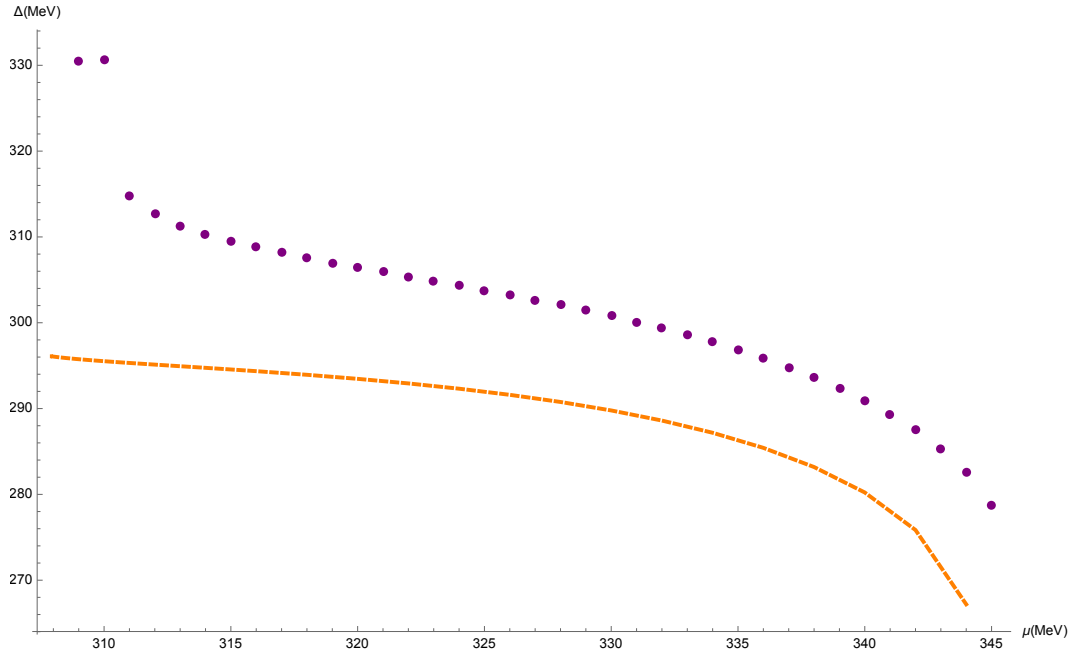

Figure 4.4: Minimization results for the 1D solitonic solution parameter Δ obtained from eq. (4.21) (dotted, purple line) compared with the results from the numerical computation (dashed, orange line) as functions of the chemical potential μ.

while for the elliptic modulus ν we have

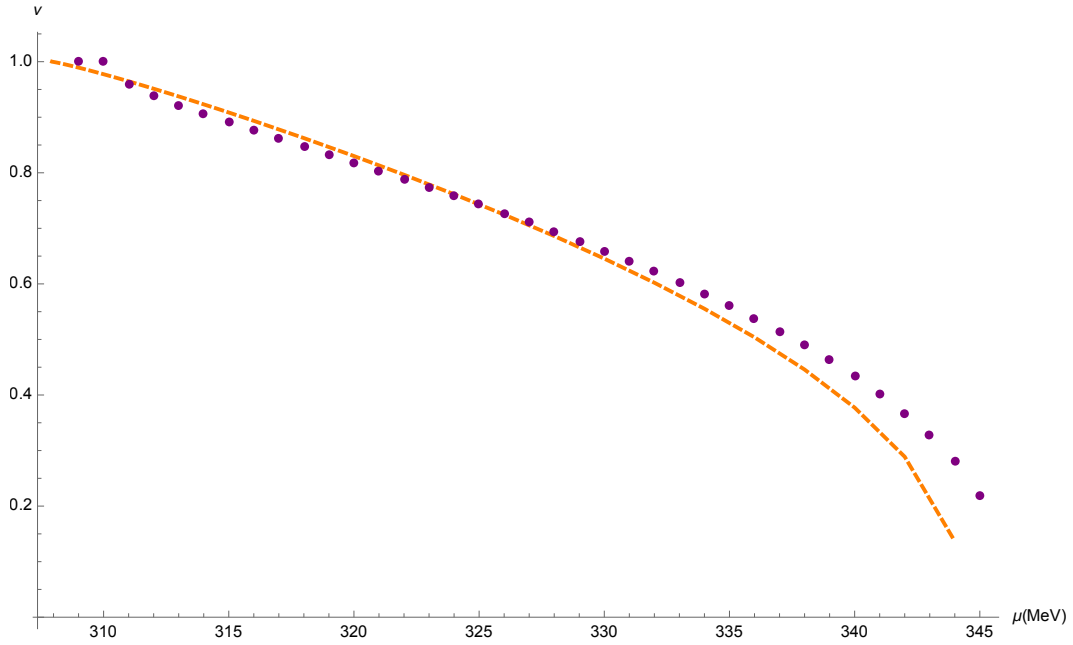

Figure 4.5: Minimization for the 1D solitonic solution parameter ν (dotted, purple line) compared with the results from the numerical computation (dashed, orange line) as functions of the chemical potential μ.

As previously discussed, these results describe parameters that are characterized by higher values with respect to the ones obtained from the numerical method.
Indeed, if we compare these results with the ones obtained in [16, 17], we can see that our Δ parameter is slightly larger: as an example, around $\mu = 310$ MeV, the numerical minimization describes an elliptic modulation with a value for $\Delta \approx 295$ MeV and a value for the elliptic modulus of $\nu \approx 0.997$. We can actually confirm in our approximation the ν minimized result, but the improved Ginzburg-Landau expansion predicts a result of $\Delta \approx 315$ MeV, which corresponds to a difference of about 5%.
The agreement that we obtained between our approximation and the numerical result for this modulation is excellent. Indeed, if we plot the differences between the restored phase and the grand potential from the numerical problem and the one derived through the improved Ginzburg-Landau expansion, we have the results in Fig 4.6

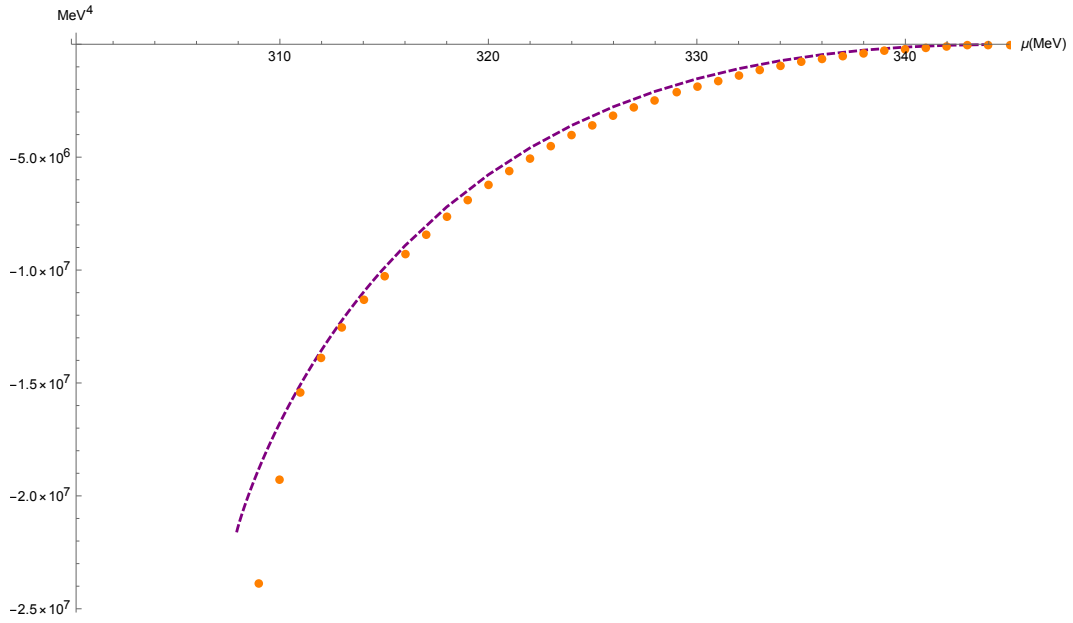

Figure 4.6: Plots of the energetic difference between the free energy for the solitonic modulation and the restored phase with the numerical computation (purple, dashed line) and with the IGL expansion (orange, dotted line) as a function of the chemical potential μ.

We can see from Figure 4.6 how our result remarkably reproduces the numerical computation results. We have to stress how the approximated result $\Omega_{TF} - \Omega_{rest}$ tends to be under $\Omega - \Omega_{rest}$, meaning that the IGL method tends to overestimate the energy gain. Nevertheless, considering how such eigenvalue problem is almost impossible to be resolved for periodic lattice structures more complicated than a plane wave or the 1D solitonic solution (even a sinusoidal order parameter cannot be resolved in an analytic way), we are allowed to say that the results obtained through the IGL method are remarkable.
In the next section, we will show how it is possible to use this method to study higher dimensional modulations.
Before doing that, we would like to report the results obtained through the improved

Ginzburg-Landau approximation for 1D sinusoidal modulation of the form

$$M_{cos}(z) = M\cos(kz). \tag{4.27}$$

and compare it with the CDW and the soliton ansatz.
Performing also the minimization with respect to the parameters M and k at different values of the chemical potential, we find the results shown in Fig 4.7

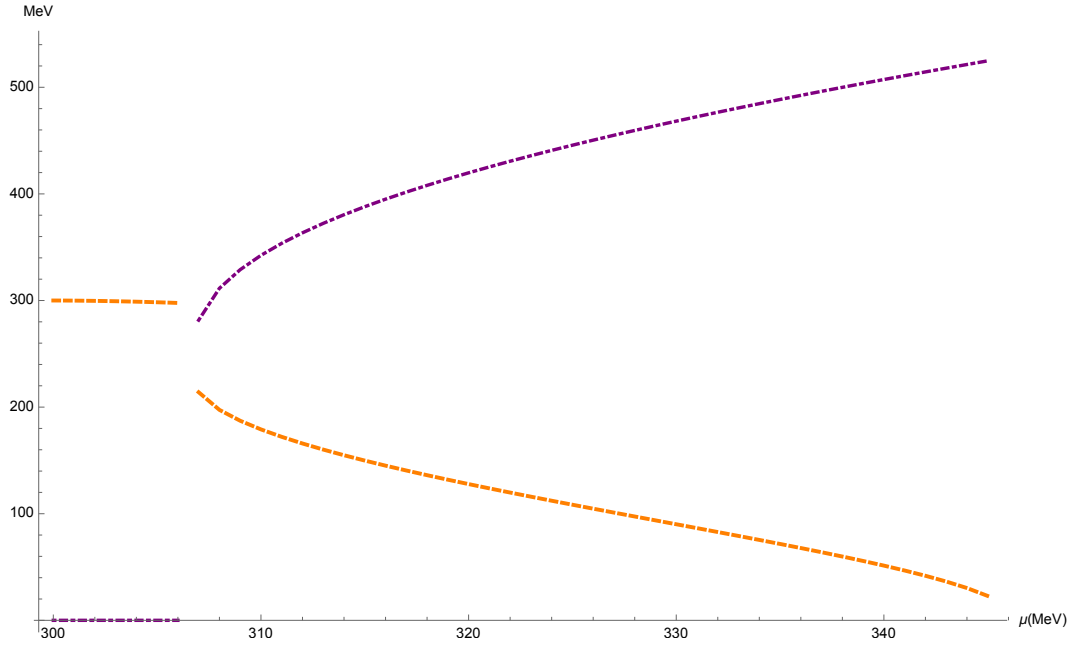

Figure 4.7: Minimized parameters for the single cosine modulation for different values of the chemical potential μ. The dashed (orange) line describes the values of the M parameter, while the dash dot line (purple) represents the k parameter.

Below the chemical potential threshold for the onset of inhomogeneous phases, we find the results characteristic for an homogeneous order parameter M: for $\mu < 308$ MeV indeed the effective mass for the condensate is minimized with a value of almost $M = 300$ MeV, while the wavevector is null. These results indeed corresponds to the well know values of the homogeneous chiral order parameter. As in the case of the CDW modulation, the critical chemical potential μ at which a modulated condensate is favored with respect to an homogeneous one is shifted of almost 3-4 MeV with respect to the numerical result. Despite the difference for the onset with the numerical computation, we are able to reproduce the results for the single cosine modulation found in [16].
Plugging the results from the numerical minimizations in the effective masses for the 1D modulations considered in this work and plotting the respective energetic differences with respect to the restored phase, we find the results in Fig 4.8

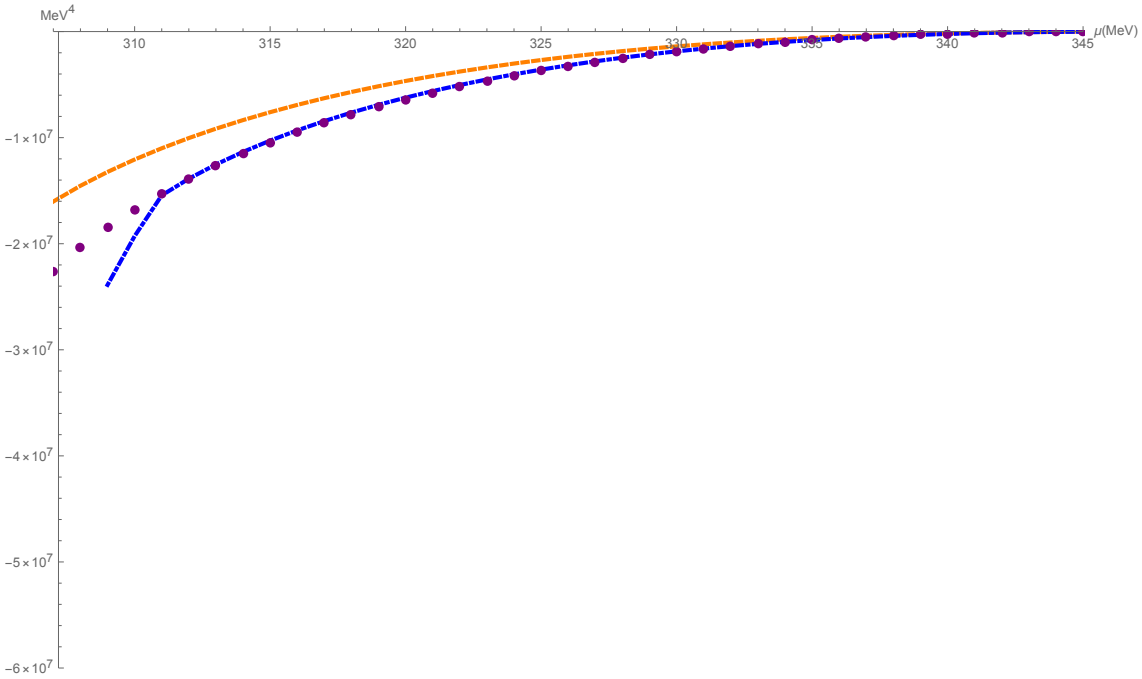

Figure 4.8: Plots of the difference between the free energies of different inhomogeneous order parameters in one dimension for different values of the chemical potential μ obtained with the IGL method and the restored phase. The dashed (orange) line describes the difference between the CDW free energy and the restored phase. The dotted (purple) line is the one-dimensional cosine free energy minus Ω_{rest}, while the dash dot (blue) line is the difference of thermodynamic potential for solitonic modulations and the free energy of the restored phase.

Through the improved Ginzburg-Landau expansion, we confirm the results found in [16, 17]: we find that the CDW modulation is disfavored both with respect to the single modulation and to the solitonic one. Furthermore, as shown by the authors in [16, 17], we confirm that the single cosine modulation is almost degenerate to the solitonic order parameter in almost all the inhomogeneous window for chiral condensates.
The success obtained with lower dimensional shapes for inhomogeneous order parameters furnishes a clear hint of the efficiency of our approximation method; in this way, on one hand we have the possibility to employ the grand potential obtained through the improved Ginzburg-Landau expansion to determine the thermodynamic properties of these phases, while on the other hand we have an analytic, simple method to deal with such phases. The lengthy and computational demanding numerical method can be replaced by a relatively simple expression for the grand potential.
It is natural to extend this method to higher dimensional modulations.

4.5 2D crystalline structures with the IGL expansion

We now want to present the results for simple two-dimensional modulations, represented by sums and products of cosines that depend on the space coordinates x and y, namely

$$\begin{aligned} M_1(x,y) &= T_1 \cos(k_1 x)\cos(k_1 y) \qquad M_2(x,y) = T_2 \cos(k_{21} x)\cos(k_{22} y), \\ M_3(x,y) &= T_3(\cos(k_3 x) + \cos(k_3 y)) \qquad M_4(x,y) = T_4(\cos(k_4 x) + \sin(k_4 y)). \end{aligned} \tag{4.28}$$

For the $M_1(x,y)$ modulation we have the possibility, again, to confront the results obtained from the improved Ginzburg-Landau expansion with the numerical results [16, 17]. After this, we will report the comparison between the thermodynamic potentials for these 2D modulation and the favored solitonic solution with respect to the restored phase.

4.5.1 $M_1(x,y)$ with IGL expansion

As already done for one-dimensional modulations, we will now present the results of the minimization of the grand potential.
In this case, the results we obtained are shown in the following Figure

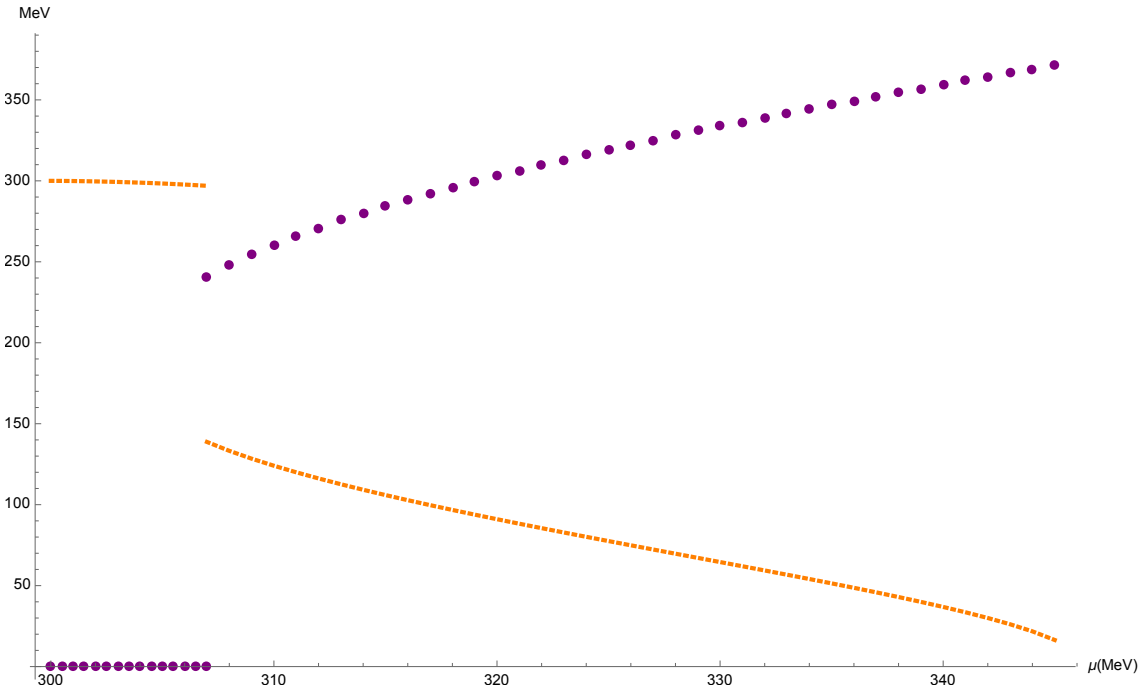

Figure 4.9: Plots of the T_1 (dashed, orange line) and k_1 (purple, dotted line) parameters of the $M_1(x,y)$ modulation that minimize the grand potential for different values of the chemical potential μ.

If we compare our results with the ones for the numerical computation shown in [17], we can see how our parameters are very close to the numerical minimization before and after the onset for inhomogeneous phases. For $\mu < 308$ MeV, our results indicate that the

optimized value for the T_1 parameter is $T_1 = 300$ MeV, which is actually the correct result for the minimization of homogeneous phases, while k_1 is null.
However, as previously seen in the case of the CDW and the 1D cosine modulations, the onset for inhomogeneous phases is predicted to be at a lower critical chemical potential ($\mu \simeq 306 - 307$ MeV) with respect to the one found by the authors in [16, 17]. Therefore, we can confirm that also for 2D structures there is a small difference of almost 3-4 MeV for the chemical potential value at which the preferred phase for the chiral condensate is inhomogeneous.
Using these values for the parameters of the $M_1(x, y)$ modulation, plugging everything inside the improved Ginzburg-Landau expansion and plotting the free energy difference between this inhomogeneous phase and the restored phase, we have the results shown in the following Figure

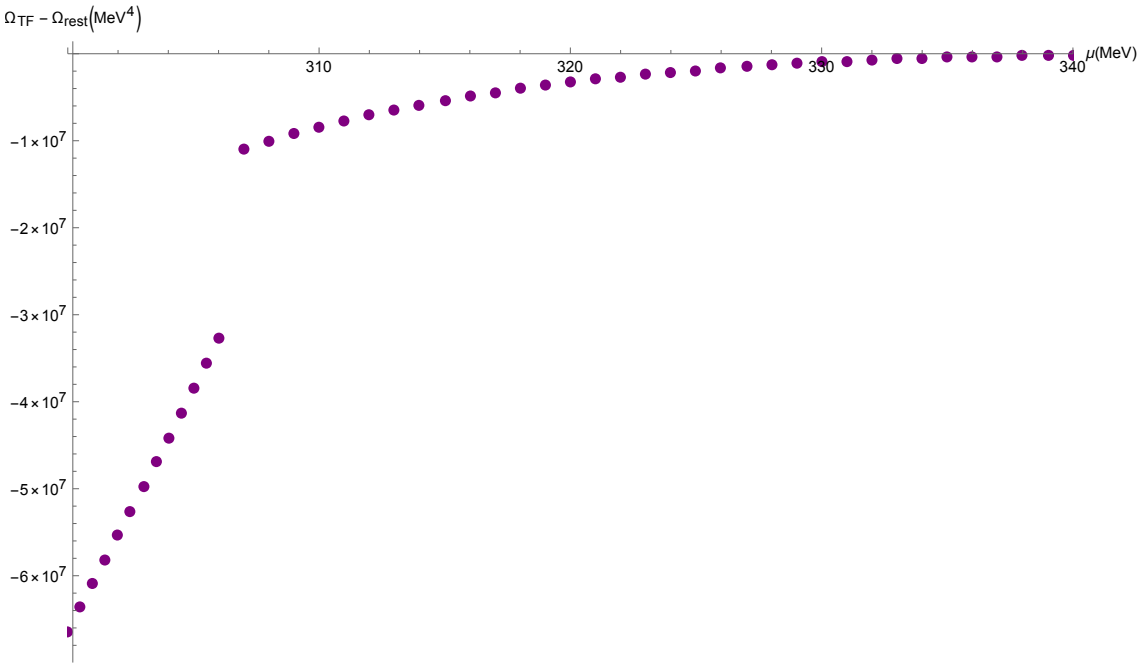

Figure 4.10: Plot of the difference between the thermodynamic potential Ω_{IGL} for the $M_1(x, y)$ modulation and the restored phase as a function of μ in the "inhomogeneous window" of the chemical potential.

If we compare the values of the energetic difference in (4.10) with the ones in [17] for the same modulation, we can see how we are able to reproduce the thermodynamic properties of this 2D modulation.

4.5.2 Comparison between different modulations

Performing the same calculation for the M_2, M_3 and M_4 proposed crystalline structures, we obtain the energy difference of the grand potential for these modulations with respect to the restored phase, and we can determine which of these forms of the chiral condensate is favored above the others shown in the following Figures. We find that there is no energy

difference between these inhomogeneous condensates. Furthermore, we compared these 2D crystalline structures with the results found for the plane wave modulation and the soliton chiral condensate. For $M_1(x, y)$ and $M_2(x, y)$ we have the results reported in Fig 4.11

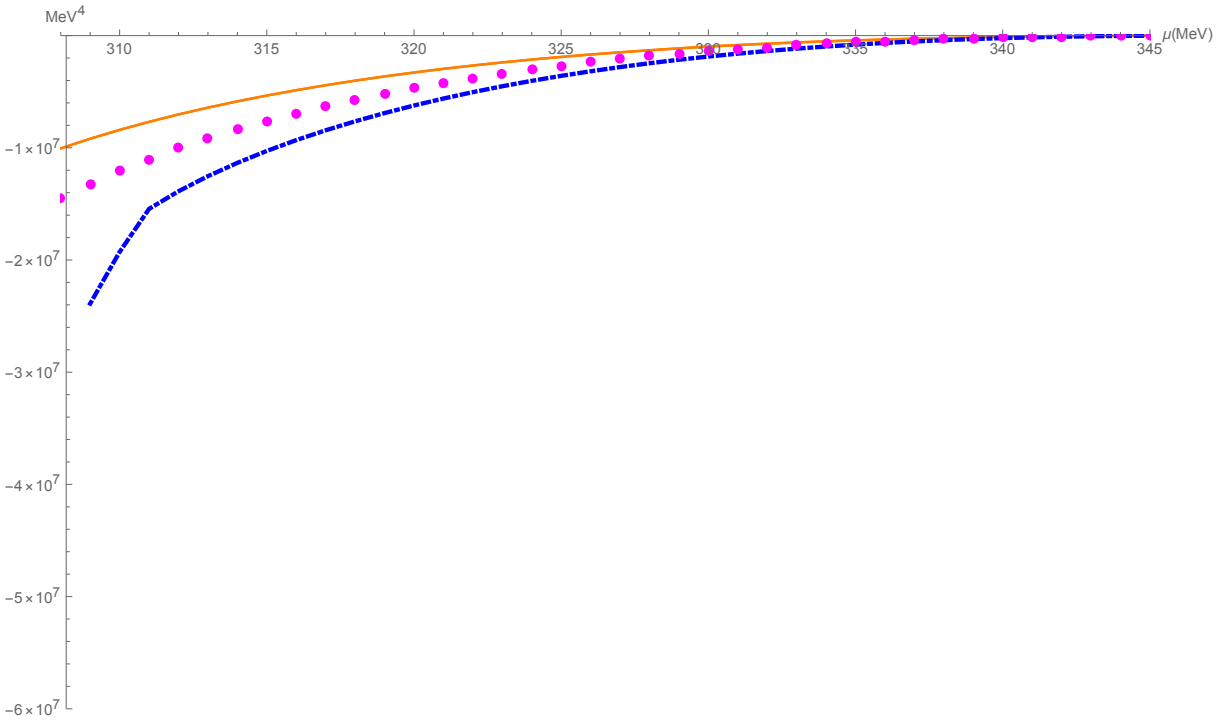

Figure 4.11: Energy difference between the thermodynamic potentials for M_1 and M_2 and Ω_{rest} solid (orange) line at different chemical potentials. The difference between the free energies of the CDW and the solitonic modulation and the restored phase are reported in dotted (magenta) and dash dot (blue) lines respectively.

From Fig 4.11, we can see how the one dimensional modulations are favored with respect to 2D lattice structures given by M_1 and M_2 throughout the inhomogeneous window.
If we compare the results of the minimizations for the parameters of $M_3(x, y)$ and $M_4(x, y)$, we have the results shown in Fig 4.12 and Fig 4.13

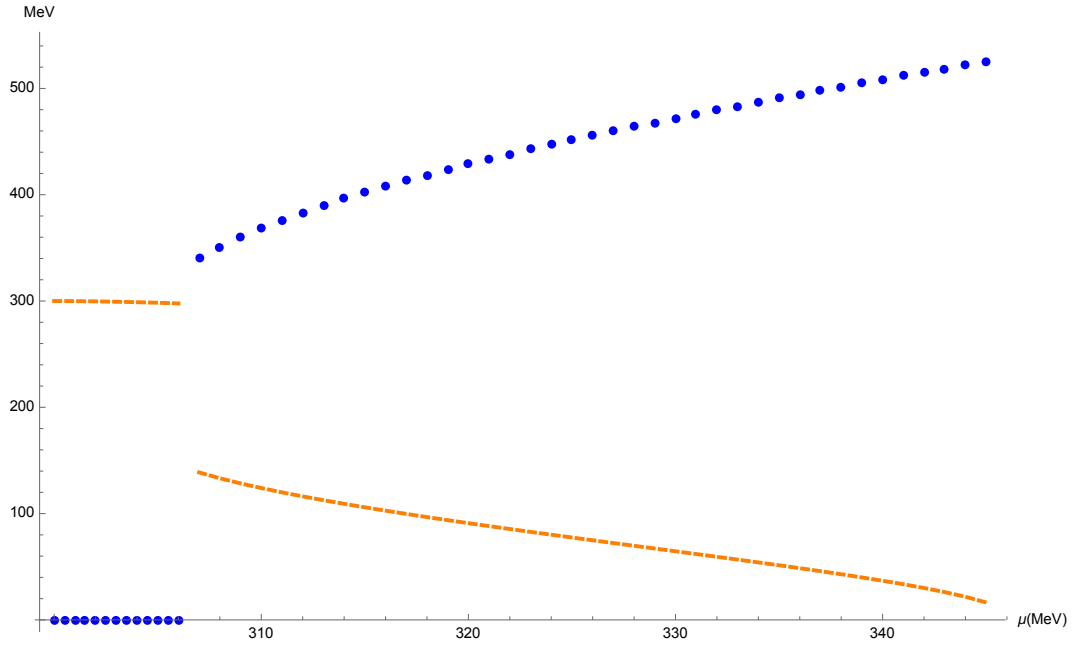

Figure 4.12: Plots of the T_3 (dashed, orange line) and k_3 (dotted, blue line) parameters of the $M_3(x, y)$ modulation that minimize the grand potential for different values of the chemical potential μ.

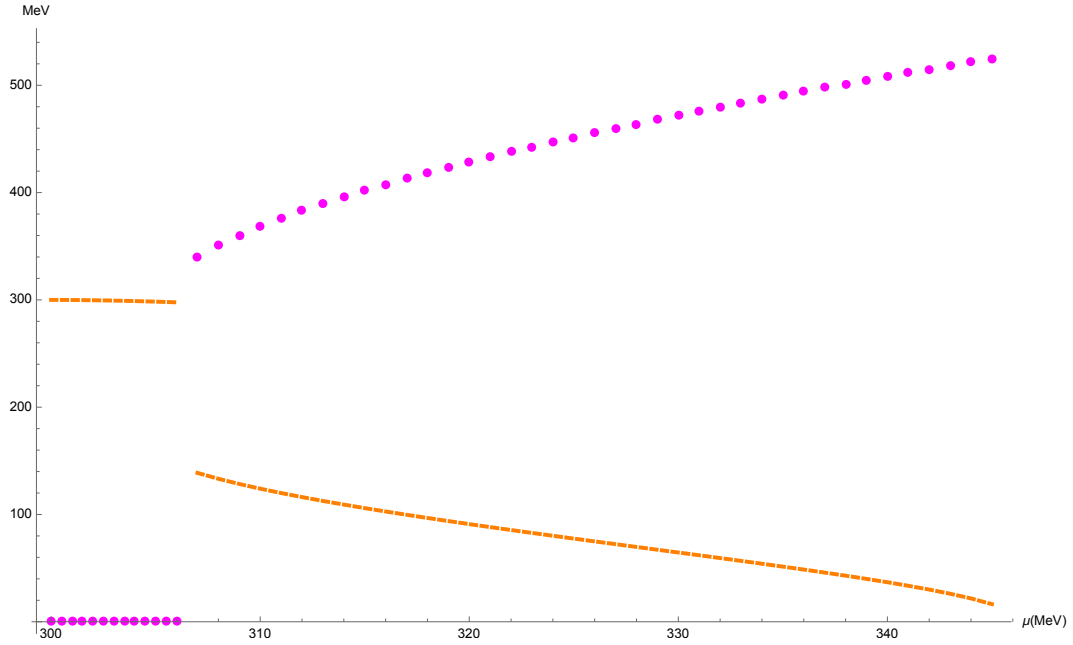

Figure 4.13: Plots of the T_4 (dashed, orange line) and k_4 (dotted, magenta line) parameters of the $M_4(x, y)$ modulation that minimize the grand potential for different values of the chemical potential μ.

It is clear from Fig 4.12 and Fig 4.13 how the two modulations have the same optimized parameters.

Plotting the free energy difference between the $M_3(x, y)$ and $M_3(x, y)$ grand potential and the restored phase, compared with the results for the CDW and solitonic modulations, we find the results in Fig 4.14

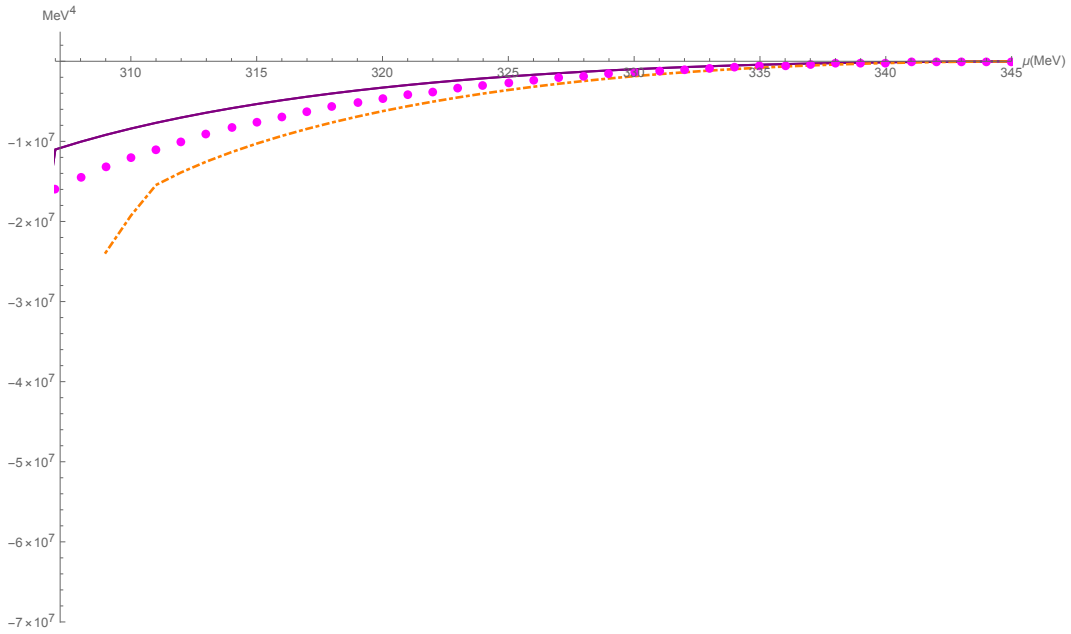

Figure 4.14: Energy difference between the thermodynamic potentials for M_3 and M_4 and Ω_{rest} at different chemical potentials (purple, solid line). The difference between the free energies of the CDW and the solitonic modulation and the restored phase are reported in dotted (magenta) and dash dot (orange) lines respectively.

We can see that from our results, in agreement with what has been previously determined [16, 17], the 1D solitonic shape for the chiral condensate is the favored one throughout the inhomogeneous window of the chemical potential which corresponds to intermediate baryonic density regions, relevant for Neutron Stars. Nevertheless, even a CDW shape for the chiral condensate is more favoured than 2D sinusoidal modulations. As already introduced, after the first order phase transition, that in our improved Ginzburg-Landau expansion occurs at 306-307 MeV, the modulations M_1, M_2, M_3, M_4 are degenerate in their energy difference from the restored phase.
We can argue that this predilection for the 1D solitonic modulation is due to the fact that the Jacobi elliptic functions are able to interpolate in a better way the transition from the homogeneous phase to the chiral restoration phase at $\mu \simeq 345$ MeV. Nevertheless, we are always adopting the mean field approximation, so we are actually neglecting the fluctuations on the top of the mean field solution. It seems, from results which are beyond the present work, that 1D modulations would be largely affected by these fluctuations, while 2D and 3D modulations would show a much more robust structure against these fluctuations [17].

Conclusions

In this work, we studied the occurrence of inhomogeneous QCD phases at zero temperature and intermediate/high baryonic potential for deconfined quark matter, which are the conditions expected in the Neutron Stars (NS) cores. We derived the explicit expression of the hamiltonian matrix for an inhomogeneous chiral order parameter in the Nambu-Jona Lasinio model, highlighting the necessity of an approximation method to describe the thermodynamic properties of inhomogeneous chirally broken phases.
We introduced a qualitative approximation for the free energy that we called the *improved Thomas-Fermi* method. In this way, we reproduced the grand potential obtained through the numerical diagonalization of the hamiltonian matrix when considering a soliton-like ansatz for the chiral order parameter. The improved Thomas-Fermi approximation allowed us to consider for the first time the competition between inhomogeneous chiral condensation and the insurgence of a modulated color superconductor in the 2SC phase in the range for the chemical potential $300 < \mu < 350$ MeV (the inhomogeneous window of the QCD phase diagram) at $T = 0$. Adopting a perturbative approach for the color superconducting order parameter, we were able to overcome the assumptions made by Sadzikowski in [8] to consider the competition between this two different phases: a 1D cosine modulation for the chiral condensate and an homogeneous 2SC color superconductor. Indeed, we found the QCD phase diagram structure obtained by different authors [1, 8, 17] but without the restriction of considering only one of the order parameters to be modulated. Proceeding in the direction of increasing chemical potential at $T = 0$, the numerical minimization of our approximate grand potential indicated the presence of a region where an inhomogeneous chiral condensate coexists with a 2SC inhomogeneous condensate, while, for increasing values of μ, we found a chiral restoration transition and an homogeneous color superconducting condensate. If on one hand we confirmed the previous results, on the other hand we enriched the QCD phase diagram structure considering the coexistence of two inhomogeneous order parameters. Moreover, our approximate approach allowed us to consider the favored soliton-like modulation for the chiral condensate [16, 17], instead of assuming a sinusoidal modulation for the sake of finding an analytic result.
After this, we rigorously derived an approximation of the grand potential for inhomogeneous, chirally broken phases of dense quark matter. We showed that it is possible to express the thermodynamic potential as the sum of a Thomas-Fermi contribution plus gradient terms which appear with the Ginzburg-Landau coefficients for a chiral density wave (CDW) modulation. Being these coefficients dependent only on the chemical potential

and the regularization scale Λ for the NJL model, we demonstrated the validity of this expansion throughout the inhomogeneous window of the chemical potential. We called this expansion the *improved Ginzburg-Landau* (IGL) method. We showed how this powerful tool can reproduce the free energy of 1D and 2D modulations with a very good approximation for every value of the chemical potential at T = 0. Indeed, we reproduced the free energies for the CDW, the solitonic and the single cosine modulations and also for known two-dimensional crystalline structures. In addition to this, we determined the grand potential for bidimensional lattice structures that couldn't be analyzed before because of the complexity of the diagonalization of the hamiltonian matrix even with numerical methods. With the IGL method we confirmed the results found in [17], where it is shown as in the mean field approximation one-dimensional modulations are favored with respect to bidimensional lattice structures. We stressed how the improved Ginzburg-Landau expansion identifies the onset for inhomogeneous phases at a lower chemical potential (around 306-307 MeV) with respect to the numerical results (which occurs at $\mu = 310$ MeV). Nevertheless, we demonstrated how the simple IGL expression for the thermodynamic potential can substitute the lengthy and almost unfeasible numerical diagonalization of the hamiltonian matrix.

The importance of the IGL model and the competition between inhomogeneous phases are due to their direct application to the physics of compact stellar objects as Neutron Stars. The recent discovery of the gravitational and the electromagnetic signals from a merger of Neutron Stars is probably the most important step toward the determination of the internal structure of NS. Despite the fact that it has been revealed the signal from only one binary system, in the near future it will be possible to compare the measures from many Neutron Stars mergers, obtaining a statistically relevant set of data that could possibly give a decisive hint on the structure of these compact objects.

Appendix A

Calculation of the grand potential for the CDW modulation

Starting from the Ω_0 term, we can integrate separately the vacuum and the medium contribution (that we have already isolated in (4.9)).
We can obtain the analytic expression for the vacuum contribution obtaining

$$\Omega_0^{vac} = -\frac{N_c N_f}{4\pi^2}\int_0^\infty dp_\perp p_\perp \int_{-\infty}^\infty dp_z \Big[E_{PV}^+ + E_{PV}^-\Big] = \frac{3}{4}\frac{N_c N_f}{4\pi^2}\Lambda^4 \log[\frac{27}{16}]. \tag{A.1}$$

For the medium contribution, we have to integrate

$$\Omega_0^{med} = -\frac{N_c N_f}{4\pi^2}\int_0^\infty dp_\perp p_\perp \int_{-\infty}^\infty dp_z \Big[(\mu - E^+), \theta(\mu - E^+) + (\mu - E^-)\theta(\mu - E^-))\Big]. \tag{A.2}$$

Taking into consideration the θ functions the integration extrema are

$$\theta(\mu - E^+) \equiv \mu > E^+ \rightarrow 0 < p_\perp < \sqrt{\mu^2 - (|p_z| + q)^2} \tag{A.3}$$

and

$$\theta(\mu - E^-) \equiv \mu > E^- \rightarrow 0 < p_\perp < \sqrt{\mu^2 - (|p_z| - q)^2}. \tag{A.4}$$

In both cases $p_\perp$ must be positive (as we already used polar coordinates for the integral over the transverse momenta).
From (A.3) we can see that μ must be such that $\mu > q$, indeed the integration domains for p_z, we get

$$E^+ \rightarrow \mu > \sqrt{(|p_z| + q)^2} \longrightarrow -\mu - q < |p_z| < \mu - q \tag{A.5}$$

and

$$E^- \rightarrow \mu > \sqrt{(|p_z| - q)^2} \longrightarrow -\mu + q < |p_z| < \mu + q. \tag{A.6}$$

In this way, we can write the medium contribution to the thermodynamic potential as

$$\Omega_0^{med} = -2\frac{N_c N_f}{4\pi^2}\Bigg\{\theta(\mu-q)\Big[\int_0^{\mu-q} dp_z \int_0^{\sqrt{\mu^2-(p_z+q)^2}} dp_\perp p_\perp(\mu - E^+) + \\ + \int_0^{\mu+q} dp_z \int_0^{\sqrt{\mu^2-(p_z-q)^2}} dp_\perp p_\perp(\mu - E^-)\Big] + \theta(q-\mu)\Big[\int_{-\mu+q}^{\mu+q} dp_z \int_0^{\sqrt{\mu^2-(p_z-q)^2}} dp_\perp p_\perp(\mu - E^-)\Big]\Bigg\}. \tag{A.7}$$

Performing both the integrations in $p_\perp$ and p_z we get

$$\Omega_0^{med} = -2\frac{N_c N_f}{4\pi^2}\Big[\theta(\mu-q)\frac{\mu^4}{6} + \theta(q-\mu)\frac{\mu^4}{6}\Big] = -\frac{N_c N_f}{12\pi^2}\mu^4. \tag{A.8}$$

In this way, we verified that actually Ω_0 corresponds to Ω_{rest}.
Now we focus on the second term of the (4.11) expansion. We have

$$\Omega_2(q) = \frac{\partial\Omega}{\partial(\Delta^2)}\Big|_{\Delta=0} = -\frac{N_c N_f}{4\pi^2}\int_0^\infty dp_\perp p_\perp \int_{-\infty}^{\infty} dp_z \sum_{\sigma=\pm}\frac{\partial\omega_\sigma}{\partial(\Delta^2)}, \tag{A.9}$$

that we can rewrite in a different way considering that

$$\frac{\partial\omega_\sigma}{\partial(\Delta^2)} = \frac{\partial\omega}{\partial(\Delta^2)} = \frac{\partial\omega}{\partial E_\sigma}\frac{\partial E_\sigma}{\partial(\Delta^2)}, \tag{A.10}$$

where

$$\frac{\partial\omega}{\partial E_\sigma} = \frac{\partial}{\partial E_\sigma}\Big(E^\sigma_{PV} + (\mu - E^\sigma)\theta(\mu - E^\sigma)\Big) = \sum_{k=0}^{3} c_k\Big(\frac{E_\sigma}{\sqrt{E_\sigma^2 + k\Lambda^2}}\Big) \\ - \theta(\mu - E_\sigma) - (\mu - E_\sigma)\delta(\mu - E_\sigma) \tag{A.11}$$

while

$$\frac{\partial E_\sigma}{\partial(\Delta^2)} = \frac{\partial}{\partial(\Delta^2)}\Big(\sqrt{p_\perp^2 + \lambda_\sigma^2}\Big) = \frac{1}{2E_\sigma}\Big(1 + \sigma\frac{q}{\sqrt{p_z^2+\Delta^2}}\Big). \tag{A.12}$$

(we recall that $\lambda_\sigma = \sqrt{p_z^2 + \Delta^2 + 2q\sigma\sqrt{p_z^2+\Delta^2}}$). In this way, we can rewrite the $\Omega_2(q)$ term as

$$\Omega_2(q) = -\frac{N_c N_f}{4\pi^2}\int_0^\infty dp_\perp p_\perp \int_{-\infty}^{\infty} dp_z \sum_{\sigma=\pm}\Bigg[\frac{1}{2E_\sigma}\Big(1 + \sigma\frac{q}{\sqrt{p_z^2+\Delta^2}}\Big)\Big(\frac{E_\sigma}{\sqrt{E_\sigma^2+k\Lambda^2}} - \\ - \theta(\mu - E_\sigma)\Big)\Bigg]. \tag{A.13}$$

We consider separately the different terms given by

$$\begin{aligned}\Omega_{2,1}^{vac} &= -\frac{N_c N_f}{4\pi^2}\int_0^\infty dp_\perp p_\perp \int_{-\infty}^{\infty} dp_z \frac{1}{2}\sum_k \frac{c_k}{\sqrt{E_\sigma^2 + k\Lambda^2}} \\ \Omega_{2,2}^{vac} &= -\frac{N_c N_f}{4\pi^2}\int_0^\infty dp_\perp p_\perp \int_{-\infty}^{\infty} dp_z \sigma \frac{q}{2\sqrt{p_z^2+\Delta^2}}\sum_k \frac{c_k}{\sqrt{E_\sigma^2 + k\Lambda^2}}\end{aligned} \tag{A.14}$$

for the two vacuum contributions emerging from the $\Omega_2(q)$ term and

$$\begin{aligned}\Omega_{2,1}^{med} &= \frac{N_c N_f}{4\pi^2}\int_0^\infty dp_\perp p_\perp \int_{-\infty}^{\infty} dp_z \frac{\theta(\mu - E_\sigma)}{2E_\sigma} \\ \Omega_{2,2}^{med} &= \frac{N_c N_f}{4\pi^2}\int_0^\infty dp_\perp p_\perp \int_{-\infty}^{\infty} dp_z \sigma \frac{q}{2E_\sigma\sqrt{p_z^2+\Delta^2}}\theta(\mu - E_\sigma)\end{aligned} \tag{A.15}$$

for the medium terms.
This time we start from the medium contributions, and remembering how the presence of the θ functions modifies the integration extrema, we can write for the $\Omega_{2,1}^{med}$

$$\begin{aligned}\Omega_{2,1}^{med} = \frac{N_c N_f}{4\pi^2}\Bigg\{&\theta(\mu-q)\Big[\int_0^{\mu-q} dp_z \int_0^{\sqrt{\mu^2-(p_z+q)^2}} dp_\perp p_\perp \frac{1}{E^+} + \\ &+ \int_0^{\mu+q} dp_z \int_0^{\sqrt{\mu^2-(p_z-q)^2}} dp_\perp p_\perp \frac{1}{E^-}\Big] + \theta(q-\mu)\Big[\int_{-\mu+q}^{\mu+q} dp_z \int_0^{\sqrt{\mu^2-(p_z-q)^2}} dp_\perp p_\perp \frac{1}{E^-}\Big]\Bigg\},\end{aligned} \tag{A.16}$$

whose result is given by

$$\Omega_{2,1}^{med} = \frac{N_c N_f}{4\pi^2}\mu^2. \tag{A.17}$$

We need to pay particular attention to the term $\Omega_{2,2}^{med}$, because we need to evaluate Ω_2 for $Q = 0$, and this term could be potentially divergent in the infrared ($p_z \simeq 0$). Nevertheless, performing the integral, we can see how actually the divergences cancel out. Indeed, for $\Delta = 0$, we see that

$$\begin{aligned}\Omega_{2,2}^{med} = q\frac{N_c N_f}{4\pi^2}\Bigg\{&\theta(\mu-q)\Big[\int_0^{\mu-q} \frac{dp_z}{p_z} \int_0^{\sqrt{\mu^2-(p_z+q)^2}} dp_\perp p_\perp \frac{1}{E^+} + \\ &+ \int_0^{\mu+q} \frac{dp_z}{p_z} \int_0^{\sqrt{\mu^2-(p_z-q)^2}} dp_\perp p_\perp \frac{1}{E^-}\Big] + \theta(q-\mu)\Big[\int_{-\mu+q}^{\mu+q} \frac{dp_z}{p_z} \int_0^{\sqrt{\mu^2-(p_z-q)^2}} dp_\perp p_\perp \frac{1}{E^-}\Big]\Bigg\}.\end{aligned} \tag{A.18}$$

If we integrate first over the transverse momenta, we obtain

$$\Omega_{2,2}^{med} = q\frac{N_c N_f}{4\pi^2}\Bigg\{\theta(\mu-q)\Big[\int_0^{\mu-q}\frac{dp_z}{p_z}\Big(\mu-\sqrt{(p_z+q)^2}\Big)- \\ -\int_0^{\mu+q}\frac{dp_z}{p_z}\Big(\mu-\sqrt{(p_z-q)^2}\Big)\Big]-\theta(q-\mu)\Big[\int_{-\mu+q}^{\mu+q}\frac{dp_z}{p_z}\Big(\mu-\sqrt{(p_z-q)^2}\Big)\Big]\Bigg\}. \tag{A.19}$$

Actually, performing the integration over p_z, $\Omega_{2,2}^{med}$ does not present any divergency in the infrared. Adopting the technique for improper integrals which present an infrared divergence, we can perform the integration considering an infinitesimal ϵ

$$\Omega_{2,2}^{med} = q\frac{N_c N_f}{4\pi^2}\Bigg\{\theta(\mu-q)\Big[\int_\epsilon^{\mu-q}\frac{dp_z}{p_z}\Big(\mu-\sqrt{(p_z+q)^2}\Big)- \\ -\int_\epsilon^{\mu+q}\frac{dp_z}{p_z}\Big(\mu-\sqrt{(p_z-q)^2}\Big)\Big]-\theta(q-\mu)\Big[\int_{-\mu+q}^{-\epsilon}\int_\epsilon^{\mu+q}\frac{dp_z}{p_z}\Big(\mu-\sqrt{(p_z-q)^2}\Big)\Big]\Bigg\}, \tag{A.20}$$

which gives

$$\Omega_{2,2}^{med} = 2q\log(q)+(\mu-q)\log\Big(\frac{\mu-q}{\epsilon}\Big)-\mu\log\Big(\frac{\mu+q}{\epsilon}\Big)-q\log[\epsilon(q+\mu)]- \\ -\mu\log\Big(\frac{\mu+q}{q-\mu}\Big)-q\log\Big(1-\frac{\mu^2}{q^2}\Big). \tag{A.21}$$

The final result is

$$\Omega_{2,2}^{med} = q\frac{N_c N_f}{4\pi^2}\Big[(\mu-q)\log\Big(\frac{|\mu-q|}{q}\Big)-(\mu+q)\log\Big(\frac{\mu+q}{q}\Big)\Big]. \tag{A.22}$$

For the integration of the vacuum contributions to Ω_2 instead we have

$$\Omega_{2,1}^{vac} = -\frac{N_c N_f}{4\pi^2}\int_{-\infty}^{\infty}dp_z\int_0^{\infty}dp_\perp p_\perp\sum_\sigma\sum_k c_k\frac{1}{2E_{\sigma,k}}\Big|_{\Delta=0} = \\ = -3\frac{N_c N_f}{8\pi^2}\Lambda^2\log\Big(\frac{4}{3}\Big) \tag{A.23}$$

while for the second we get

$$\Omega_{2,2}^{vac} = q\frac{N_c N_f}{4\pi^2}\int_0^{\infty}dp_z p_z\sum_\sigma\sum_k\sigma c_k\sqrt{(p_z+\sigma q)^2+k\Lambda^2} \\ = -q\frac{N_c N_f}{4\pi^2}\sum_k c_k\Big[(q-\sqrt{q^2+k\Lambda^2})\log(k\Lambda^2)+2\sqrt{q^2+k\Lambda^2}\log(q+\sqrt{q^2+k\Lambda^2})\Big]. \tag{A.24}$$

Eventually, we can write

$$\begin{aligned}\Omega_{2,1}^{vac} &= -3\frac{N_c N_f}{8\pi^2}\Lambda^2 \log\Big(\frac{4}{3}\Big),\\ \Omega_{2,2}^{vac} &= -q\frac{N_c N_f}{4\pi^2}\sum_k c_k\Big[(q-\sqrt{q^2+k\Lambda^2})\log(k\Lambda^2)+2\sqrt{q^2+k\Lambda^2}\log(q+\sqrt{q^2+k\Lambda^2})\Big],\end{aligned} \tag{A.25}$$

while for the medium part

$$\begin{aligned}\Omega_{2,1}^{med} &= \frac{N_c N_f}{4\pi^2}\mu^2,\\ \Omega_{2,2}^{med} &= q\frac{N_c N_f}{4\pi^2}\Big[(\mu-q)\log\Big(\frac{|\mu-q|}{q}\Big)-(\mu+q)\log\Big(\frac{|\mu+q|}{q}\Big)\Big].\end{aligned} \tag{A.26}$$

Appendix B

Quantum Chromodynamics-basics

Quantum Chromodynamics (QCD) is the non-abelian gauge theory of strong interactions. The charge associated to the gauge group is called *color*. If Quantum Electrodynamics is described by the $U(1)$ abelian group, the symmetries of strong interactions are described by a $SU(3)_{color}$ non abelian group. The $SU(3)_{color}$ generators do not commute, and this allocates a color charge to the force carriers, which are the *gluons*, the gauge bosons of QCD.
For each flavor, three possible color states are allowed for each quark

$$q^f(x) = \begin{bmatrix} q^f_r(x) \\ q^f_g(x) \\ q^f_b(x) \end{bmatrix}. \tag{B.1}$$

This color triplet transforms under local-color transformation of $SU(3)$ as

$$q^f(x) \longrightarrow q'^f(x) = U_c(x) q^f(x). \tag{B.2}$$

A generic local *finite* transformation is expressed through an exponential form

$$U_c(x) = exp[i\alpha_S \theta^a(x) G_a], \tag{B.3}$$

whose infinitesimal expression is given by

$$exp[i\alpha_S \theta^a(x) G_a] \simeq \mathbb{1} + i\alpha_S \theta^a(x) G_a. \tag{B.4}$$

where α_S is the coupling constant, a = 1,...,8 are the color indices and G_a are the group generator conventionally expressed as

$$G_a = \frac{\lambda_a}{2}, \tag{B.5}$$

where λ_a are the Gell-Mann (3x3) matrices. Furthermore, they verify the commutation relation

$$[G_a, G_b] = i f_{abc} G_c \tag{B.6}$$

(f_{abc} are the group structure constants).
In order to achieve local gauge invariance, the *gluon* gauge bosons must be introduced, which are the massless mediators of the strong force. Adopting the standard notation for such gauge fields, they will be denoted as $A_a(x)$. For local gauge invariance, is necessary to include in the Lagrangian a term which would describe free gluons and, in addition, the ordinary derivative must be modified including the minimal coupling with the gauge fields

$$D_\mu = \partial_\mu + i\alpha_S A^a(x) G_a. \tag{B.7}$$

Inserting this expression in the kinetic term for quarks we get

$$\mathcal{L} = \sum_{a,b,f} q^f(x)_a i\gamma^\mu [D_\mu]_{ab} q^f(x)_b. \tag{B.8}$$

Requiring local gauge invariance one obtains that

$$A^a_\mu \longrightarrow A'^a_\mu = A^a_\mu - \partial_\mu \theta^a(x) - \alpha_S f^{abc} \theta_b A_{c,\mu} \tag{B.9}$$

and including the kinetic term for free gauge bosons in the Lagrangian we get

$$\mathcal{L} = \sum_f q^f(x)_a i\gamma^\mu [D_\mu]_{ab} q^f(x)_b - \frac{1}{4} G^a_{\mu\nu} G^{\mu\nu}_a \tag{B.10}$$

where $G^{\mu\nu}_a$ stands for the non abelian analogue of the Maxwell tensor for Electrodynamics. Its expression is given by

$$G^a_{\mu\nu} = \partial_\nu A^a_\mu - \partial_\mu A^a_\nu + i\alpha_S [A_\mu, A_\nu]. \tag{B.11}$$

Summarizing, the query for invariance under local color transformations led us to the introduction of gauge boson whose transformation properties guarantee such request. The striking difference between QCD and QED is that the force carriers have a color charge. This implies that quantum chromodynamics is characterized by gluons interactions among themselves.
We now would like to outline the basic notions necessary for the description of the most elementary interactions in QCD as representative examples of how quantum chromodynamics works among quarks and antiquarks.

Quark-antiquark interaction

Let us consider an up quark and down antiquark interacting through the exchange of a gluon.
In the fundamental representation for the quarks, the product of a quark and an antiquark is given by a color singlet or an octet state

$$\mathbf{3} \otimes \mathbf{3} = \bar{\mathbf{1}} \oplus \mathbf{8}.$$

Applying the Feynman rules to a couple belonging to an octet state formed by R-antiG quarks for example, because of color conservation, the outcome would be again a pair R-antiG. The Feynman amplitude is given by

$$\begin{aligned} -i\mathcal{M} = &\Big[\bar{u}(3)c_3^\dagger\big(-i\alpha_S\frac{\lambda_a}{2}\gamma^\mu\big)u(1)c_1\Big]\times\Big[-i\frac{g_{\mu\nu}\delta_{ab}}{q^2}\Big] \\ &\Big[\bar{v}(2)c_2^\dagger\big(-i\alpha_S\frac{\lambda_b}{2}\gamma^\nu\big)v(4)c_4\Big], \end{aligned} \tag{B.12}$$

where

$$c_1 = c_3 = \begin{bmatrix}1\\0\\0\end{bmatrix} \qquad\qquad c_2 = c_4 = \begin{bmatrix}0\\1\\0\end{bmatrix}$$

which are vectors indicating the quarks-antiquarks colors.
The attractive/repulsive action of the gluon exchange depends on the *color factor*, whose sign is determined by the Gell-Mann matrices elements that appear in the Feynman amplitude and by the color-vectors.
For an octet state we have

$$c_F = \frac{1}{4}\Big[c_3^\dagger\lambda^\alpha c_1\Big]\Big[c_4^\dagger\lambda^\alpha c_2\Big] = \frac{1}{4}\lambda^\alpha_{11}\lambda^\alpha_{22} = -\frac{1}{6} \tag{B.13}$$

Indeed, for an octet state, we have a repulsive force between the quark and the antiquark. On the other hand, considering a singlet state given by

$$\frac{1}{\sqrt{3}}\Big(R\bar{R} + G\bar{G} + B\bar{B}\Big) \tag{B.14}$$

the outcome of the interaction would be in general a pair **color**-anticolor (as B-antiB for example). In this case, the color factor is

$$c_F = \frac{1}{12}Tr\Big(\lambda^\alpha\lambda^\alpha\Big) = \frac{4}{3} \tag{B.15}$$

Being the color factor positive, the resulting force in the singlet channel is attractive.

Quark-quark interaction

We start taking in consideration two quarks. Since quarks are in the fundamental representation, their product can be an antitriplet or a sextet

$$\mathbf{3}\otimes\mathbf{3} = \bar{\mathbf{3}}\otimes\mathbf{6}.$$

An example of an antitriplet is given by

$$\frac{1}{\sqrt{2}}(GB - BG),$$

which of course is antisymmetric, while a symmetric state (sextet) could be expressed as

$$\frac{1}{\sqrt{2}}(RB + BR),$$

or

$$GG.$$

Considering a color sextet state, the Feynman amplitude of the process would be given by

$$\begin{aligned} -i\mathcal{M} = &\Big[\bar{u}(3)c_1^\dagger\big(-i\alpha_S\frac{\lambda_a}{2}\gamma^\mu\big)u(1)c_3\Big] \times \Big[-i\frac{g_{\mu\nu}\delta_{ab}}{q^2}\Big] \\ &\Big[\bar{u}(2)c_2^\dagger\big(-i\alpha_S\frac{\lambda_b}{2}\gamma^\nu\big)u(4)c_4\Big], \end{aligned} \tag{B.16}$$

while considering a triplet state we would get

$$\begin{aligned} -i\mathcal{M} = &\Big[\bar{u}(3)c_1^\dagger\big(-i\alpha_S\frac{\lambda_a}{2}\gamma^\mu\big)u(1)c_3\Big] \times \Big[-i\frac{g_{\mu\nu}\delta_{ab}}{q^2}\Big] \\ &\Big[\bar{u}(2)c_2^\dagger\big(-i\alpha_S\frac{\lambda_b}{2}\gamma^\nu\big)u(4)c_4\Big], \end{aligned} \tag{B.17}$$

where we have indicated the color vectors as

$$c_r = \begin{bmatrix}1\\0\\0\end{bmatrix}, \qquad c_g = \begin{bmatrix}0\\1\\0\end{bmatrix}, \qquad c_b = \begin{bmatrix}0\\0\\1\end{bmatrix},$$

which specify the color orientation in color space of the quarks. With q instead indicates the momentum of the gluon.

The attractive/repulsive action of the gluon exchange depends, again, on the *color factor*, whose sign is determined by the Gell-Mann matrices elements that appear in the Feynman amplitude and by the color-vectors of the interacting particles.
For qq interactions, a repulsive force is exerted in the sextet channel (*color factor* >0), while an attractive one in antitriplet channel (*color factor* <0), because the potential is given by

$$V_{qq} = c_F\frac{\alpha_S}{r}. \tag{B.18}$$

Appendix C

Gran Canonical Ensemble

In quantum regimes, the Gran Canonical ensemble allows for variations of the total number of particles of the considered system. Such fluctuations swing around the mean value of particles $\bar{N}$.
The Gran Canonical distribution is deduced considering a subsystem S which can exchange energy and particles with a reservoir. When looking at the complete system (S + reservoir), in conclusion, the total energy and the number of particles is fixed.
In order to define the distribution which could describe the thermodynamics of the subsystem S, the starting point is considering the probability that the subsystem is found in the infinitesimal phase space volume $\mathrm{d}\Gamma_s$.
Subsequently, we obtain the sought distribution

$$Z_{GC} = \sum_N \frac{e^{\frac{\mu N}{k_B T}}}{N! h^{3N}} \int dp^{3N} dq^{3N} e^{-\frac{E}{k_B T}}, \tag{C.1}$$

where Z_C is the canonical partition function.
All the relevant thermodynamic quantities can be determined through Z_{GC}. Indeed, considering a system whose particle number fluctuations are negligible we can write

$$Z_{GC} = \sum_N e^{\frac{\mu N}{\tau}} Z_C \simeq e^{\frac{\mu \bar{N}}{\tau}} \bar{Z_C} = e^{\frac{\mu \bar{N} - F(T,V,\bar{N})}{k_B T}}, \tag{C.2}$$

where $F(T, V, \bar{N})$ stands for the Helmholtz free energy.
The thermodynamic potential for the grand canonical ensemble is given by

$$\Omega = F - \mu N \tag{C.3}$$

where μ is the chemical potential. Expressing it in its differential form we get

$$d\Omega = dF - d(\mu N) = -SdT - pdV - Nd\mu. \tag{C.4}$$

Subsequently, we can determine the physical quantities that describe the system

$$\Big(\frac{\partial\Omega}{\partial T}\Big)_{V,\mu} = -S; \qquad \Big(\frac{\partial\Omega}{\partial V}\Big)_{T,\mu} = -p; \qquad \Big(\frac{\partial\Omega}{\partial \mu}\Big)_{T,V} = N;$$

where S indicates the entropy of the system, p its pressure and N is the number of particles. From (C.2) we can see that if we express

$$\Omega = -k_B T ln(Z_{GC}) \tag{C.5}$$

we can deduce all the information required to describe the system.
We now want to show how the Gran Potential is actually the pressure when divided for the volume of the system. We introduce the Gibbs thermodynamic potential (which is an extensive quantity)

$$G = F + pV \longrightarrow dG = -SdT + Vdp + \mu dN. \tag{C.6}$$

Being an additive quantity, we can express G as

$$G(T, p, N) = Ng(T, p) \tag{C.7}$$

and

$$\mu = \Big(\frac{\partial G}{\partial N}\Big)_{T,p} = g(T, p) \longmapsto G = \mu N. \tag{C.8}$$

Eventually,

$$\Omega = F - \mu N = G - pV - \mu N = -pV. \tag{C.9}$$

Bibliography

[1] M. Buballa *NJL-model analysis of dense quark matter* (https://arxiv.org/abs/hep-ph/0402234v2), 27 Jan 2005

[2] F. Wilczek, K. Rajagopal *The Condensed Matter Physics of QCD* (https://arxiv.org/abs/hep-ph/0011333v2), 13 Dec 2000

[3] M. G. Alford, A. Schmitt *Color superconductivity in dense quark matter* (10.1103/RevModPhys.80.1455), 11 Nov 2008

[4] I. A. Shovkovy *Two lectures on color superconductivity* (https://arxiv.org/abs/nucl-th/0410091v2), 8 Nov 2004

[5] J. A. Bowers *Color Superconducting Phases of Cold Dense Quark Matter* (https://arxiv.org/abs/hep-ph/0305301v1), 27 May 2003

[6] V. Koch *Aspects of Chiral Symmetry* (https://arxiv.org/pdf/nucl-th/9706075.pdf), 27 Jun 1997

[7] R. Anglani, R. Casalbuoni, M. Ciminale, R. Gatto, N. Ippolito, M. Mannarelli, M. Ruggieri *Crystalline color superconductors* (https://arxiv.org/abs/1302.4264v2), 12 Apr 2014

[8] M. Sadzikowski *Coexistence of pion condensation and color superconductivity in two flavor quark matter* (https://arxiv.org/abs/hep-ph/0210065v2), 13 Jun 2003

[9] S. L. Shapiro, S. A. Teukolsky *Black holes, White Dwarfs, Neutron Stars* (DOI: 10.1002/9783527617661), 29 Dec 2007

[10] C. A. van Eysden, A. Melatos. *Pulsar glitch recovery and the superfluidity coefficients of bulk nuclear matter* (https://arxiv.org/abs/1007.4360v1), 25 Jul 2010

[11] B. Haskell, N. Andersson, C. D' Angelo, N. Degenaar, K. Glampedakis, W. C.G. Ho, P. D. Lasky, A. Melatos, M. Oppenoorth, A. Patruno, M. Priymak *Gravitational waves from rapidly rotating neutron stars* (https://arxiv.org/abs/1407.8254v1), 31 Jul 2014

[12] C. A. van Eysden, A. Melatos. *Gravitational radiation from pulsar glitches* (https://arxiv.org/abs/0809.4352v1), 25 Sep 2008

[13] Y. Nambu, G. Jona Lasinio. *Phys. Rev.* ***122***, 345 (1961)

[14] Y. Nambu, G. Jona Lasinio. *Phys. Rev.* ***124***, 246 (196x)

[15] D. Nickel. *Inhomogeneous phases in the Nambu-Jona Lasino and quark-meson model* (https://arxiv.org/abs/0906.5295v1), 29 Jun 2009

[16] S. Carignano. *Inhomogeneous chiral symmetry breaking phases* (PhD thesis), 2012

[17] S. P. Klevansky *The Nambu-Jona Lasinio model of quantum chromodynamics* (https://arxiv.org/pdf/1406.1367), 7 Oct 2014

[18] M.Buballa, S. Carignano *Inhomogeneous chiral condensates* (Rev. Mod. Phys. 64, 649), 1 Jul 1992

[19] J. I. Kapusta, C. Gale *Finite-temperature filed theory, Principles and Applications* (Cambridge Monographs on mathematical physics), Second edition, 2006

[20] M. Kutschera, W. Broniowski, A. Kotlorz *Quark matter with pion condensate in an effective chiral model* Nuclear Physics, **A516**, 566-588 , 26 March 1990

[21] G. Başar, G. V. Dunne *A Twisted Kink Crystal in the Chiral Gross-Neveu model* (https://arxiv.org/abs/0806.2659v2), 11 Sep 2008

[22] S. Maedan *Influence of Current Mass on the Spatially Inhomogeneous Chiral Condensate* (https://arxiv.org/abs/0908.05940), 18 Dec 2009

[23] M. Huang *Color Superconductivity at Moderate Baryon Density* (https://arxiv.org/abs/hep-ph/0409167v2), 4 Nov 2004

[24] J. Berges, K. Rajagopal *Color Superconductivity and Chiral Symmetry Restoration at Nonzero Baryon Density and Temperature* (https://arxiv.org/abs/hep-ph/9804233), 14 Sep 1998